Hydrothermal conversion of mixed uranium(IV)–cerium(III) oxalates into U_1 − −x Ce_xO_2+δ

×

nH_2O solid solutions

Sofian Benarib, Nicolas Dacheux, X. F Le Goff, J. Lautru, Lara Di Mascio, Nicolas Clavier

Dalton Transactions

ROYAL SOCIETY OF CHEMISTRY

PAPER

View Article Online
View Journal | View Issue

Cite this: *Dalton Trans.*, 2023, **52**, 10951

Hydrothermal conversion of mixed uranium(IV)–cerium(III) oxalates into $U_{1-x}Ce_xO_{2+\delta}{\cdot}nH_2O$ solid solutions†

S. Benarib, N. Dacheux, X. F. Le Goff, J. Lautru, L. Di Mascio and N. Clavier *

Uranium–cerium oxide solid solutions, $U_{1-x}Ce_xO_{2+\delta}{\cdot}nH_2O$, were prepared through hydrothermal conversion of mixed U(IV)–Ce(III) oxalate precursors, cerium being used as a surrogate for plutonium. Whatever the starting pH, the fluorite-type structure of AnO_2 was obtained after heating at 250 °C for 24 h. The initial pH of the reaction media appeared to affect significantly the oxide morphology: for pH ≤ 2, the powder was found to be composed of microspheres, whereas for more alkaline pH values, agglomerates of nanocrystallites were found. Furthermore, a study of the hydrothermal treatment duration (T = 250 °C, pH = 8, t = 1–48 h) showed that fluorite-type mixed dioxides started to form after only 1 h, and then became single phase after 3 h. SEM and TEM/EDS analyses revealed that the cationic distribution narrowed with time to finally form highly homogeneous mixed oxides. Such a preparation route was then applied to various cerium incorporation rates and it was found that the formation of $U_{1-x}Ce_xO_{2+\delta}{\cdot}nH_2O$ mixed oxides was possible for $0.1 \leq x \leq 0.75$. In all the systems investigated, the speciation of uranium and cerium was questioned in both the solid and liquid phases. Thermodynamic calculations and evaluation of the O/M ratio in the final oxides led us to understand the complex redox behaviour of uranium and cerium in solution during hydrothermal processes and to propose a conversion mechanism.

Received 20th May 2023,
Accepted 13th July 2023

DOI: 10.1039/d3dt01510f

rsc.li/dalton

1. Introduction

Among several objectives, the development of new generations of nuclear power plants aims at increasing the reactor safety and at saving uranium resources, mainly through an effective closing of the nuclear fuel cycle. In this frame, MOx fuels, *i.e.* mixed uranium–plutonium oxides, enable the use of recycled resources coming from the reprocessing of UOx spent fuels,[1] along with reducing the waste volume and toxicity. In parallel, the plutonium content within MOx is expected to increase in Gen-III and Gen-IV fuels, compared with that currently operating in pressurized water reactors (PWRs). Nowadays, MOx fuel is prepared through a powder metallurgy process and is composed of about 92% of depleted uranium and 8% of plutonium. Yet, the so-obtained oxides contain Pu-enriched agglomerates that could limit their use inside future Gen-IV reactors.[2] Indeed, such a heterogeneous distribution of cations can cause hotspots during the fuel's stay in the reactor and complicate its dissolution in the eventuality of MOx fuel reprocessing. It is then compulsory to set up advanced fuel reprocessing schemes and subsequent refabrication processes that can adapt to these new constraints.

As an answer, wet chemistry routes have been studied for the fabrication of mixed oxide fuels such as $(U,Pu)O_2$ (MOx). They are frequently based on the precipitation of low-temperature precursors and present the advantage of improving the homogeneity of the cation distribution[2,3] and enhancing the resistance towards proliferation. Most of these studies focus on oxalic precipitation,[4] because it allows the direct and quantitative precipitation of precursors and generally yields solid solutions,[5–7] which can be converted into oxides after heat treatment at high temperature.[8–13] Nevertheless, such wet chemistry routes are not free from drawbacks, among which is the presence of residual carbon within the samples that can lead to dedensification during sintering[14] or to an oxide morphology inherited from the precursor.[15]

Alternatively, recent studies have been devoted to the hydrothermal conversion of various An(IV) (Th, U, Np, Pu) oxide precursors, as a more compact conversion process. During hydrothermal conversion, the low-temperature compound is decomposed, thanks to the temperature and autogenous pressure, possibly releasing metal cations in solution. The latter are then possibly complexed by anions, precipitated and aged

ICSM, Univ Montpellier, CEA, CNRS, ENSCM, Marcoule, France.
E-mail: nicolas.clavier@icsm.fr; Fax: +33 4 66 79 76 11; Tel: +33 4 66 33 92 08

† Electronic supplementary information (ESI) available. See DOI: https://doi.org/10.1039/d3dt01510f

further into hydrated oxide. Using urea,[16] aspartate[17,18] or oxalate[9,19–21] as a complexant, it is possible to precipitate directly and quantitatively hydrated oxides from ions in solution under mild conditions ($T \leq 250$ °C). Typically, uranium oxide can be obtained through the hydrothermal conversion of U(IV) oxalate after 1 h at 250 °C,[20] whereas thorium oxide is synthesised after treating $Th(C_2O_4)_2{\cdot}6H_2O$ for at least 5 h by keeping all other parameters constant.[19] The syntheses of many single and mixed oxides have already been achieved this way, such as UO_2,[20–22] ThO_2,[19,21,22] PuO_2,[21,22] NpO_2,[21] $(U,Th)O_2$,[21,23] $(U,Pu)O_2$,[21,24] $(Np,Pu)O_2$,[21] $(Th,Pu)O_2$,[21] $(Th,U,Np)O_2$ and $(Th,Np,Pu)O_2$.[23] Nevertheless, hydrothermal conversion of systems with actinide and/or lanthanide cations exhibiting different oxidation states remains scarce and has been only reported by Vigier *et al.*,[25] who synthesised recently $(U,Am)O_2$ and $(U,Pu,Am)O_2$.

In this context, this article is focused on the direct preparation of $U_{1-x}Ce_xO_{2+\delta}$ solid solutions through hydrothermal conversion of U(IV)–Ce(III) mixed oxalates. Herein, cerium acts as a surrogate for plutonium, owing to its several similar properties including the cationic radius and stabilized oxidation states in the solid and solution states.[26–29] The U–Ce–O system displays complex behaviour due to the redox properties of uranium and cerium in solution and in the solid state.[26] Indeed cerium can be tri- or tetravalent, while uranium can be present in the oxidation states of +IV, +V or +VI in solid oxide phases.

To gain insight into the consequences of this complex redox interplay on the hydrothermal conversion process, a multi-parametric study was undertaken, including the effects of pH, the duration of hydrothermal treatment and the chemical composition of the mixed oxalate. In this work, oxides were synthesised by converting oxalates through hydrothermal routes and afterwards the samples were characterised thoroughly to study the evolution of their physicochemical properties. First, ICP-OES analyses allowed the determination of the precipitation yield as well as the sample stoichiometry after acid digestion. Then, the structure was investigated through XRD analysis, while the morphology was studied using scanning and transmission electronic microscopies. The homogeneity of the cation distribution within the samples was assessed by means of SEM-EDS and TEM-EDS analyses. Finally, the presence of residual carbon or water in samples was checked using a carbon analyser and thermogravimetric analysis.

The optimal conditions for the hydrothermal conversion of oxalates into oxides are reported herein. Also, the conversion mechanism is discussed through the study of cation behaviour in solution and redox evolution during the hydrothermal conversion.

2. Experimental

2.1. Sample preparation

All the reagents used were of analytical grade and supplied by Sigma-Aldrich, except for uranium metal chips kindly supplied by CETAMA. On the one hand, the uranium(IV) solution was prepared by dissolving these metal pieces in hot concentrated hydrochloric acid. Metal chips were rinsed with dichloromethane, acetone, and water and then washed with 2 mol L^{-1} HCl to eliminate uranium oxide which could have been formed at the surface of the metal. Finally, 6 mol L^{-1} HCl was used to dissolve the uranium metal chips, leading to a final concentration close to 0.6 mol L^{-1}. Thanks to the high chloride concentration, the tetravalent state of uranium was maintained for several months in solution.[30] On the other hand, cerium(III) nitrate hexahydrate was dissolved in water to prepare the initial cerium precursor solution with a concentration close to 0.4 mol L^{-1}.

All the samples studied in this work were prepared through the precipitation of mixed cerium(III) and uranium(IV) oxalates. The amounts of uranium (n_U) and cerium (n_{Ce}) were adjusted by mixing the stock solutions in order to obtain the targeted molar ratio in the final mixed oxide $U_{1-x}Ce_xO_{2\pm\delta}$ (with $x = n_{Ce}/(n_{Ce} + n_U)$), with a total cation concentration of 26 mmol L^{-1}. This mixture was poured in a 50 mol% excess of 0.5 M oxalic acid in an aqueous solution, leading to the formation of a pinkish-grey powder precipitate. As the resulting media was very acidic (typically pH < 1), the pH value was adjusted to the desired value by adding ammonia (30 mass% Carlo Erba commercial solution). Thereafter, the solid phase and the supernatant were transferred in a 23 mL Teflon-lined autoclave (4749 Acid Digestion Vessel – Parr). The mixed oxide composition targeted in this article is $U_{0.8}Ce_{0.2}O_{2+\delta}$, except in the variation of the oxide stoichiometry section. This latter was chosen to study a composition between that of the current MOx and that of the master blend.

The temperature of the hydrothermal treatment has been shown to strongly impact the hydrothermal conversion mechanism and thus the properties of the as-obtained oxide. A previous study carried out by our team[20] showed that syntheses must be carried out at 250 °C, in order to achieve quantitative cationic precipitation and to minimise the presence of impurities within the final oxides. Therefore, this temperature was fixed for every syntheses reported herein.

Whatever the experimental conditions tested, the volume of the solution was adjusted to 15 mL to avoid any bias induced by a change of autogenous pressure. According to the diagram reported by Rabenau,[31] for an autoclave heated at 250 °C with a filling factor "*f*" of 65% (*i.e.* $f = \frac{15\text{ mL}}{23\text{ mL}} \approx 0.65$), the pressure is expected to be around 60 bars when the autoclave is heated at 250 °C. The as-obtained mixed oxalates were then converted into oxide samples under mild hydrothermal conditions.

3. Sample characterisation

3.1. ICP-OES measurements

In order to evaluate the precipitation yields, supernatants were separated from the solid after hydrothermal conversion by centrifugation (14 500 rpm, 5 min). ICP-OES measurements

(ICP-AES Spectro Arcos) were then performed. Intensities of the emission peaks were recorded at λ = 385.958 and 409.014 nm for uranium and λ = 404.076 and 535.353 nm for cerium. To calibrate the apparatus, a set of standard solutions was prepared, starting from 1000 ppm standard solutions purchased from SCP Science, with concentrations ranging from 0.5 to 15 ppm. The analysed solutions were diluted in order to present a concentration included in the calibration range and therefore to measure the concentration by interpolation.

Then, in order to check the chemical composition of the solid phases obtained after hydrothermal conversion, 5 mg of each sample were mixed with 10 mL of aqua regia, and then placed in a PTFE reactor. The reactors were finally loaded into an Ethos Easy microwave digestion platform (purchased from Milestone) to achieve full dissolution of the compounds at 225 °C for 40 min. The solutions obtained were finally diluted and analysed by the means of ICP-OES.

3.2. PXRD

Powder X-ray diffraction (PXRD) patterns were recorded using a Bruker D8 diffractometer equipped with a LynxExe detector adopting the Bragg–Brentano geometry and using Cu $K\alpha_{1,2}$ radiation (λ-$K\alpha_1$ = 1.54060 Å; λ-$K\alpha_2$ = 1.54439 Å). Data acquisitions were performed at room temperature, with 2θ varying from 5° to 90° with a step size of 0.01° and a total counting time of 205 minutes. Unit cell parameters and average crystallite sizes were refined by the Rietveld method with GSAS-II software[32] using CIF files downloaded from the Crystallography Open Database (COD ID: 1541648) corresponding to mixed uranium–cerium oxides.

3.3. Microscopic observation (SEM, TEM, and EDS)

Powder morphologies were observed using scanning electron microscopy. Powders were deposited on carbon adhesive tape, without any additional preparation. A FEI Quanta 200 scanning electron microscope equipped with an Everhart–Thornley detector (ETD) and a back-scattered electron detector (BSED) was used to record micrographs at an acceleration voltage of 15 kV under high vacuum conditions (10^{-6} Pa). To assess cationic homogeneity within the prepared oxides, X-EDS was performed with a SEM device using a Bruker XFlash 5010 detector. Furthermore, TEM micrographs were obtained using a JEOL 2200FS-200 kV high-resolution transmission electron microscope (HR-TEM) at the MEA platform (University of Montpellier). Additionally, STEM-EDS analyses were obtained on an Oxford Instrument X-MaxN 100 TLE EDX detector with a spot size of 0.7 nm.

3.4. Carbon analyses

The residual carbon content in the mixed oxide powders prepared by hydrothermal conversion was determined with a LECO CS230 carbon/sulfur analyser by the complete combustion under an oxygen atmosphere and CO_2 concentration measurement by IR absorption. To remove adsorbed atmospheric CO_2, the samples were first dried overnight at 90 °C in an oven. At least three measurements were performed on the samples to obtain reliable values and to estimate associated uncertainties. Blanks and series of high purity steel reference materials (containing 0.06 to 2.32 wt% in carbon) were analysed right before the samples to calibrate the analyser.

3.5. FTIR spectroscopy

Fourier-transform infrared spectra were recorded in the 615–4000 cm^{-1} range using a PerkinElmer FTIR Spectrum 100 apparatus. Samples were deposited at the surface of an ATR crystal after being ground manually with a mortar and a pestle. The collected spectrum exhibited a resolution of 2 cm^{-1}.

3.6. TG-MS analyses

Thermogravimetric analyses were performed under a reductive atmosphere (Ar/H_2-4%) on a Setsys Evolution Setaram apparatus. After recording a baseline using an empty crucible, the weight loss was measured during a heat treatment up to 1000 °C with a heating rate of 5 °C min^{-1}.

4. Results

4.1. Effect of initial pH

4.1.1. Precipitation yield and chemical composition. Since uranium(IV) and cerium(III) present different chemical behaviours in solution, especially towards hydrolysis, pH has been chosen as the first parameter to be studied. In this aim, five different values were selected to be set as the starting pH of the reacting mixture before hydrothermal conversion (*i.e.* 2, 4, 5.5, 8 and 10), which covers a large range where $U(OH)_4$, $Ce(OH)_3$ and $Ce(OH)_4$ species could be formed. To quantify the precipitation yield of cations, ICP-OES analyses have been carried out on the supernatants collected both after the oxalic precipitation of the precursors and their subsequent hydrothermal conversion (Table 1). These measurements highlight the quasi-quantitative precipitation of uranium and cerium

Table 1 Variation in the uranium and cerium precipitation yields and the composition of the initial oxalate and oxide obtained after hydrothermal treatment (T = 250 °C, t = 24 h) as a function of the initial pH (expected cation composition of 80 mol% uranium and 20 mol% cerium for all the samples)

	Uranium precipitation yield (%)	Cerium precipitation yield (%)	U/(U + Ce) molar ratio[a] (%)	Ce/(U + Ce) molar ratio[a] (%)
Initial oxalate	95 ± 2	98 ± 2	79 ± 2	21 ± 2
2	96 ± 2	96 ± 2	77 ± 2	23 ± 2
4	98 ± 2	97 ± 2	77 ± 2	23 ± 2
5.5	97 ± 2	97 ± 2	78 ± 2	22 ± 2
8	97 ± 2	98 ± 2	81 ± 2	19 ± 2
10	98 ± 2	99 ± 2	79 ± 2	21 ± 2

[a] Molar ratios determined from concentrations measured in solution after full dissolution in aqua regia.

under the chemical conditions studied, with global precipitation yields systematically above 95% (after the initial oxalic precipitation) or 96% (after hydrothermal treatment). The U/(U + Ce) cationic ratios measured (Table 1) are in good agreement with the expected values and confirm the quasi-quantitative yield of precipitation observed in the whole pH range. As such, the pH did not seem to affect strongly the precipitation yield of the cations, and thus the final composition of the oxide synthetized by hydrothermal conversion, at least under the conditions studied (*i.e.* T = 250 °C and t = 24 h). This result could appear surprising as $U(OH)_{4\ (s)}$,[33] $Ce(OH)_{3\ (s)}$ or $Ce(OH)_{4\ (s)}$[34,35] are not supposed to form at acidic pH under atmospheric conditions. Indeed, according to Bouchaud *et al.*[34] and calculations from the data of Hayes *et al.*,[36] $Ce(OH)_{3\ (s)}$ is supposed to form only from pH = 8 and become the predominant cerium species in solution above pH = 10 ([Ce] = 0.1 mol L^{-1}, 25 °C, $pO_2 = 2.1 \times 10^4$ Pa simulating an aerated solution at room temperature). On the other hand, calculations carried out by Opel *et al.*[37] for uranium showed that $U(OH)_{4\ (aq)}$ starts to form around pH = 4 and becomes the predominant uranium hydroxide species around pH = 5.5. As oxide compounds are very often obtained through the ageing of such hydroxide species during the hydrothermal conversion process,[11] the behaviours of both uranium and cerium, and particularly hydrolysis equilibria, were strongly affected by hydrothermal conditions. Hence, temperature and autogenous pressure allowed the quasi-quantitative and congruent precipitation of both uranium and cerium during the hydrothermal conversion of mixed oxalate into oxide on the whole pH range studied.

4.1.2. Structural characterisation of the samples. XRD analyses were then carried out both on the sample obtained from the initial oxalic precipitation step and on powders obtained after hydrothermal conversion (Fig. 1). Oxalic precipitation led to the formation of uranium–cerium mixed oxalate, as XRD lines match well with those reported by Tamain *et al.*[38] for $(NH_4)_x[(Pu_x^{+III}U_{1-x}^{+IV}(C_2O_4)_2)H_2O]\cdot nH_2O$ solid solutions. By analogy, our sample was identified as $(H_3O)_x[(Ce_x^{+III}U_{1-x}^{+IV}(C_2O_4)_2)\cdot H_2O]\cdot nH_2O$, *i.e.*, as a mixed U(+IV)–Ce(+III) oxalate, in which the charge compensation is ensured by the hydronium cation.

XRD patterns of oxide samples prepared by hydrothermal conversion of the oxalate precursor at different pH values are presented in Fig. 1b. The characteristic fluorite-type structure ($Fm\bar{3}m$) of U[39] and Ce[40,41] dioxides is obtained whatever the pH studied. Moreover, after 24 hours of hydrothermal treatment, no XRD peak characteristic of the oxalate precursor can be detected, meaning that the initial U(+IV)–Ce(+III) oxalate precursor has been fully decomposed. Additionally, no extra peak characteristic of the sesquioxide Ce_2O_3 is present. Cerium being in the trivalent oxidation state in the initial oxalate, this indicates that cerium is oxidised, at least partly, during the hydrothermal treatment. A few peaks might appear on a random basis, around 2θ = 21° and 28°, and are caused by the presence of small amounts of orthorhombic M_3O_8[42,43] (M = U and Ce), originating from the partial oxidation of U(IV) during the hydrothermal treatment.

Following the Rietveld refinement of XRD data, Fig. 2a shows no evident change of the unit cell volume for pH ≤ 5.5, with values ranging from 160.45 to 160.59 Å^3. In the same time, the crystallites obtained are nanometric with an average size ranging from 15 to 47 nm. Nevertheless, for oxides obtained under alkaline conditions (*i.e.* pH = 8 and 10), the Rietveld method leads to better results when two contributions are considered during the refinement procedure. Indeed, one can note that starting from pH = 8, the peak profiles are different, as shown in the insets in Fig. 1. The difference is quite noticeable for the sample prepared at pH = 10, where two contributions are necessary to fit the peak profile. It is important to note that the centroids of the two peaks are very close, almost overlaid, which results in the absence of peak splitting. This particular peak profile arises from the fact that the two contributions used for the fit present different widths, corresponding to a variation of the crystallite size within the sample. In addition, the small shift between the centroids can be explained either by a slight difference in terms of cerium content, or by a difference in the oxygen stoichiometry (*i.e.*, O/M ratios).

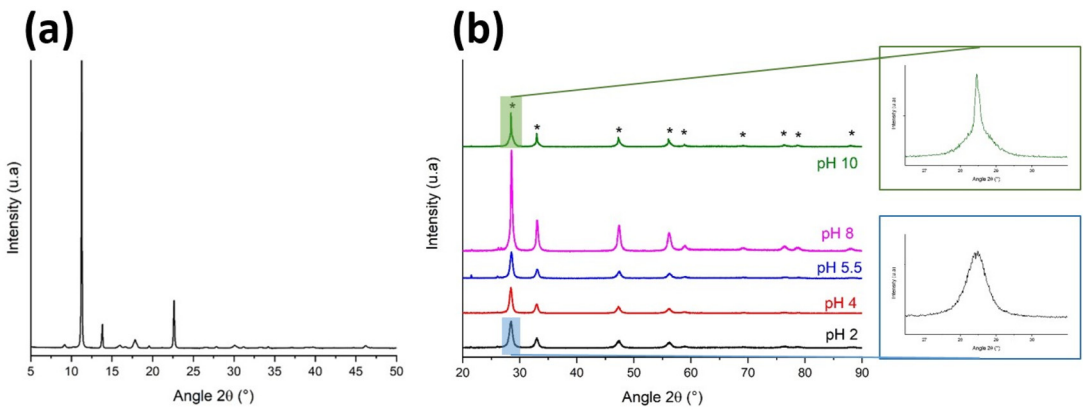

Fig. 1 (a) XRD pattern obtained for the initial mixed uranium–cerium oxalate (b) and variation in the XRD patterns obtained for samples prepared by hydrothermal conversion from pH = 2 to pH = 10 (T = 250 °C, t = 24 h). Asterisks correspond to the XRD lines of $U_{0.79}Ce_{0.21}O_2$ reported in ref. 44.

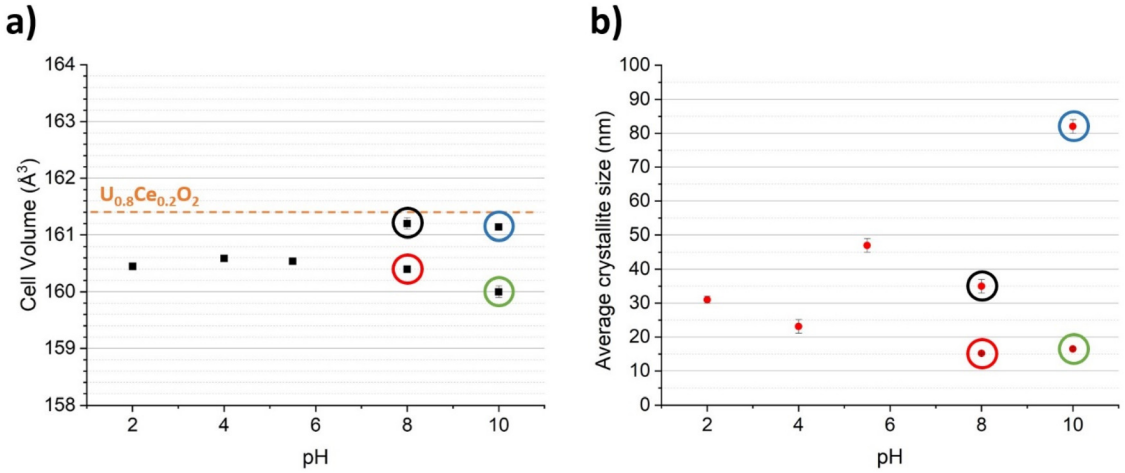

Fig. 2 Variation in (a) the unit cell volumes calculated for our samples with that reported by Cao *et al.*[45] for $U_{0.8}Ce_{0.2}O_2$ in orange; (b) average crystallite size of mixed uranium–cerium oxide as a function of initial pH (T = 250 °C, t = 24 h). The most and less crystallised populations are circled in black (wt% = 10%) and red (wt% = 90%), respectively, for pH = 8, and in blue (wt% = 40%) and green (wt% = 60%) for pH = 10.

Hence, two cell volumes and crystallite sizes are reported in Fig. 2 for pH 8 and 10. In both cases, populations exhibiting smaller crystallites present a similar cell volume (160.4 ± 0.1 Å^3 for pH = 8 and 160.0 ± 0.1 Å^3 for pH = 10) and an average crystallite size under 20 nm (*i.e.* 15.2 ± 0.2 nm and 16.5 ± 0.3, respectively). This could indicate that the smallest crystallites within the sample present a larger O/M ratio, as a result of their higher reactivity towards oxidation. On the other hand, populations exhibiting larger crystallites present similar cell volumes (161.2 ± 0.1 Å^3 and 161.14 ± 0.02 Å^3 for pH = 8 and 10, respectively) but quite different average crystallite sizes. Indeed, from 35 ± 2 nm for pH = 8, it increased up to 82 ± 2 nm at pH = 10.

Another information obtained from Rietveld refinements is the weight fraction of the two populations. The weight content associated with the phase exhibiting the largest crystallites size is always the lower within the oxide, meaning that nucleation is favoured. In this field, the population with the largest crystallites represents only 10% of the total (circled in black in Fig. 2) for pH = 8 and increases to 40% for pH 10 (circled in blue in Fig. 2). Two contributions are needed to properly refine the XRD pattern corresponding to pH = 10. Nevertheless, for pH = 8, the diagram can be fairly refined with one contribution. Indeed, owing to the similar unit cell volumes obtained for the two populations at pH = 8, only one contribution will be finally used to refine XRD diagrams of the samples prepared in the following sections of this study.

4.1.3. Homogeneity of the prepared samples. The composition of the oxide samples was first quantified thanks to their full dissolution in acid solution followed by ICP-OES measurements. Complementary SEM-EDS analyses were then carried out to quantify the homogeneity of cation distribution. The powder samples obtained after hydrothermal treatment were first shaped into pellets in order to present a flat surface and therefore to avoid any bias coming from the sample topology. Two areas were selected on each pellet surface with fifty data points were collected in each zone. The electron beam–matter interaction droplet volume was about 1 μm^3. Considering the particle size calculated previously (around 30 nm), this volume accounted for many crystallites, and only heterogeneities with a size larger than 1 μm were detected. As a matter of comparison, Pu-enriched agglomerates in typical MOX fuels can be up to 50 μm in diameter.[2]

By drawing an histogram to represent the cerium content (with the bin size set as 0.5%), the distribution was systematically found to follow a normal law, which was fitted with a Gaussian curve. As such, several statistic parameters like the distribution centre x_c and $\sigma = \frac{\text{full width at half maximum}}{2\sqrt{\ln(4)}}$ were determined. Hence, the x_c value could be given with a 2σ confidence level which includes 95% of the datapoints collected. On this basis, the 2σ value was chosen to assess the cationic homogeneity within the oxide, as the SEM-EDS analyses were shown to be only semi-quantitative. As such, Fig. 3 presents the normalised 2σ dispersion as a function of pH, namely the 2σ value for each pH studied, divided by the average cerium content measured with SEM-EDS analyses, expressed in at.% of cations. It shows that cerium distribution is narrow whatever the pH studied, roughly around ±5% of the normalized cerium content. Moreover, the orange area presented in Fig. 3 allows comparing the homogeneity of the samples with that of an oxide sample prepared by thermal conversion of the same precursor (6 h at 1000 °C under an Ar/H_2-4% atmosphere). For the latter, 95% of the values were also included in a ±5% interval, meaning that the cationic homogeneity was close for these two synthesis routes. Overall, for all studied pH values, the hydrothermal conversion (T = 250 °C, t = 24 h) of U(IV)/Ce(III) oxalates allows the synthesis of homogeneous oxide based solid solutions.

4.1.4. Morphology of the samples. SEM micrographs were recorded on all the samples prepared in order to evidence the variation of the morphology after the hydrothermal conversion

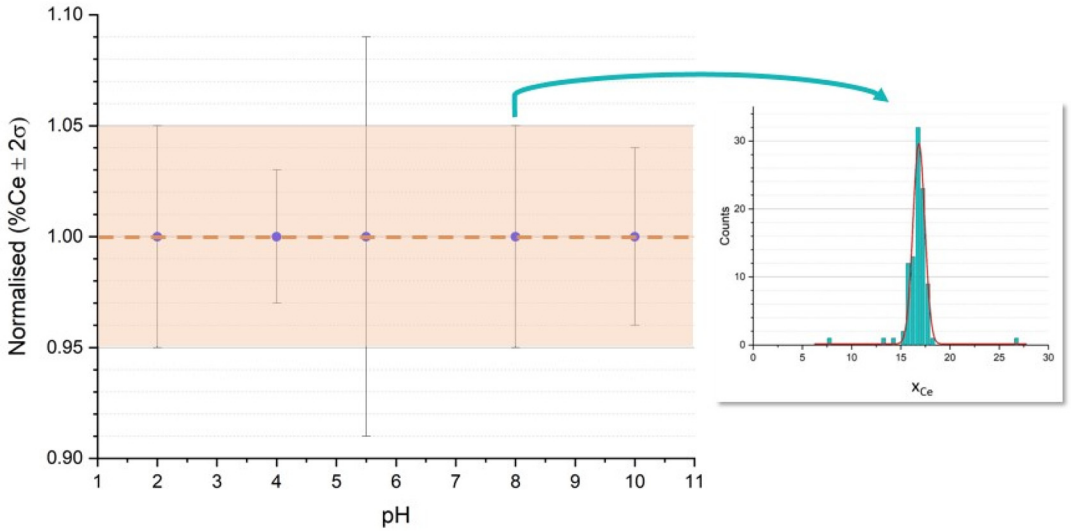

Fig. 3 Variation in the cationic homogeneity within the oxides obtained by the hydrothermal conversion of oxalates as a function of the initial pH. The inset shows the statistical analysis of the oxide prepared at pH = 8. The orange area shows the homogeneity obtained for an oxide prepared by thermal treatment (T = 1000 °C, t = 6 h, Ar/H_2-4% reducing atmosphere).

of oxalates into oxides (Fig. 4). The initial precursor presents the characteristic platelet-like morphology of An(IV) oxalates, already evidenced by several authors.[46,47] The platelets obtained present homogeneous size, around 3 μm. The oxide sample prepared by heat treatment of the precursor presents a similar morphology that highlights the pseudo-morphic char-

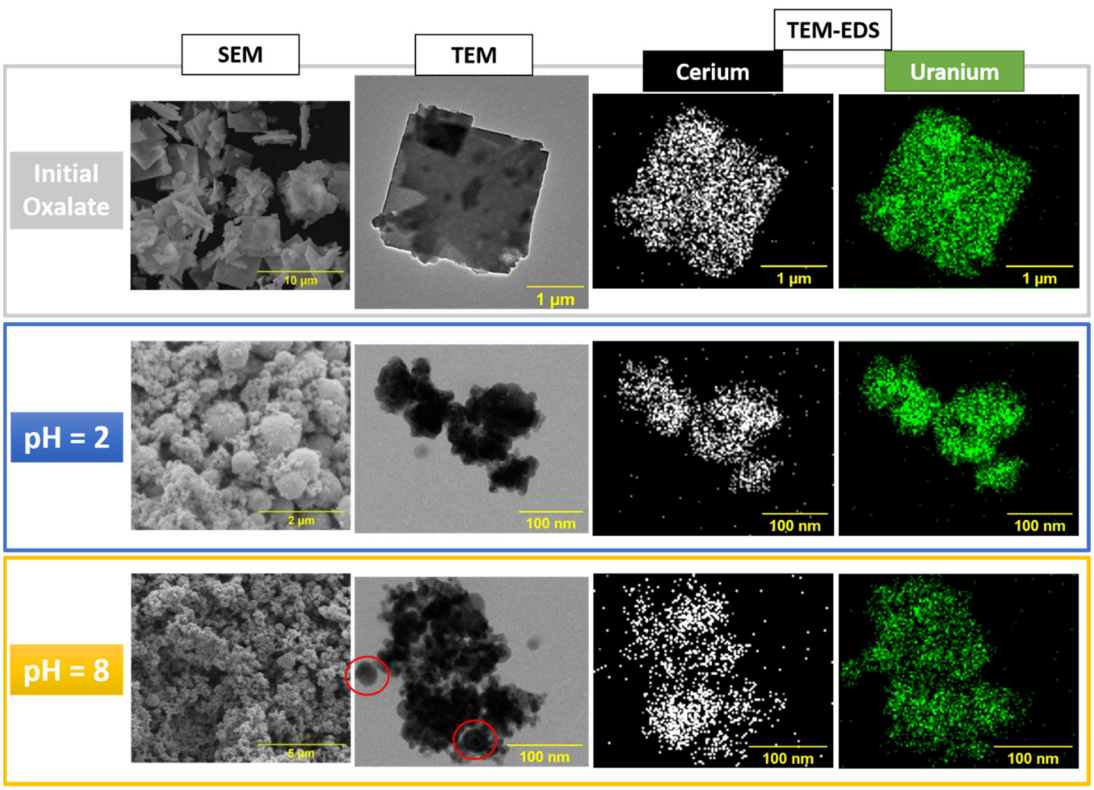

Fig. 4 SEM (SE mode) and TEM micrographs obtained for the initial mixed uranium cerium oxalate and oxides obtained after hydrothermal treatment (T = 250 °C, holding time = 24 hours) with various starting pH values. Crystallites exhibiting larger size are circled in red. TEM-EDS analyses carried out on initial oxalate and oxides obtained after hydrothermal treatment (T = 250 °C, t = 24 h) with various starting pH values (white and green dots stand for cerium and uranium signals, respectively).

acter of the oxalate–oxide thermal conversion, which could impact in return the flowability of the powder and therefore its behaviour during shaping and sintering processes[14] (see the micrograph in Fig. S1† supplied as a complementary material).

Meanwhile, the hydrothermal conversion allowed us to tune the morphology of the final oxide samples. Indeed, after 24 hours of hydrothermal treatment at 250 °C and with pH = 2, the powder was found to be composed of spherical agglomerates of about 1 μm in diameter. Such a modification in terms of morphology has been already described by several authors.[17,23,48,49] Recent studies[50–52] have explained these results from controlled self-assembly phenomena, not by classical crystal growth, but rather through complex mechanisms binding nanocrystallite units and controlled by organic species present in solution. For instance, Manaud *et al.* synthesised thorium[19] and uranium[20] oxides exhibiting a similar spherical morphology from the hydrothermal conversion of actinide oxalates under acidic conditions, typically at pH = 2. Trillaud *et al.*[18] also converted uranium(IV) aspartate into uranium dioxide through hydrothermal treatment and obtained spherical agglomerates at pH = 3. In our study, for pH = 5, oxide samples present a heterogeneous morphology with microspheres and agglomerates of crystallite with a size not exceeding 50 nm. On the other hand, above pH = 8, the oxide morphology is solely composed of the agglomerates of nanocrystallites. Once again, these results are in good agreement with those obtained by Manaud *et al.* for uranium oxide[20] and thorium oxide.[19]

Additional TEM observations confirmed the existence of nanometric crystallites, with a size around a dozen of nanometers (Fig. 4), which is compatible with the value calculated from Rietveld refinements. The small discrepancy between the calculated and observed sizes can be explained by the fact that the average crystallite size obtained from the XRD data can be affected by the largest crystallites, scarcely observed on TEM micrographs (as an illustration, some large crystallites are circled in red in Fig. 4).

In order to qualitatively investigate the homogeneity of the cationic distribution in the samples at the nanoscale, complementary TEM-EDS analyses were carried out (Fig. 4). TEM-EDS micrographs obtained for the initial oxalate show that the precursor is homogeneous, in good agreement with the precipitation of a single-phase oxalate solid solution evidenced by XRD. In a similar way, TEM micrographs recorded for the oxide sample prepared at pH = 2 or pH = 8 show that every crystallites contain uranium and cerium. This is clearly illustrated for a crystallite secluded at the far-left of the micrograph. These results complement previous XRD and SEM-EDS analyses, as they confirm that the oxides obtained after hydrothermal treatment are homogeneous solid solutions and not assemblies of separated UO_2 and CeO_2, even for basic conditions of conversion.

4.1.5. Carbon and water contents in the prepared samples. Impurities within the oxides prepared by hydrothermal conversion of oxalate precursors mainly consist of residual carbon and water. Their content was evaluated by chemical analysis and TGA experiments, respectively (Table 2). They show that the carbon content slightly varies as a function of the pH of the initial mixture, with values ranging from 0.20 to 0.52 wt%. It is worth noting that these values are higher than those observed for uranium oxides obtained through the hydrothermal conversion of oxalates, which are typically below 0.1 wt%.[20] This might indicate the presence of organic species coming from the decomposition of the oxalate precursor.

Table 2 Carbon (wt%) and water (mol mol^{-1} cation) contents determined in the oxides obtained by the hydrothermal conversion of oxalate (T = 250 °C, t = 24 h) for various starting pH values

Initial pH	Carbon (wt%)	mol H_2O/mol cation
2	0.35 ± 0.05	0.4 ± 0.1
4	0.27 ± 0.05	0.6 ± 0.1
5.5	0.30 ± 0.05	0.6 ± 0.1
8	0.52 ± 0.05	0.6 ± 0.1
10	0.20 ± 0.05	0.4 ± 0.1

Indeed, complementary FTIR analyses (Fig. 5) performed on these oxides show that carbon remaining in the samples after conversion is existing as carboxylate groups resulting from the decomposition of the oxalate precursor. Several vibration bands arise from the presence of carboxylate groups: first, the intense band at 900 cm^{-1} can be attributed to the ν_s symmetric stretching of CO coupled with in-plan-bending O–C=O and scissoring δ O–C=O. Then, at 1072 cm^{-1} a weak signal can be assigned to the COO rocking and C–H out of plane bending, as described by Nakamoto[53] or Ito.[54] The signal at 1380 cm^{-1} is caused by COO rocking and C–H in-plan bending, once again characteristic of carboxylate groups.

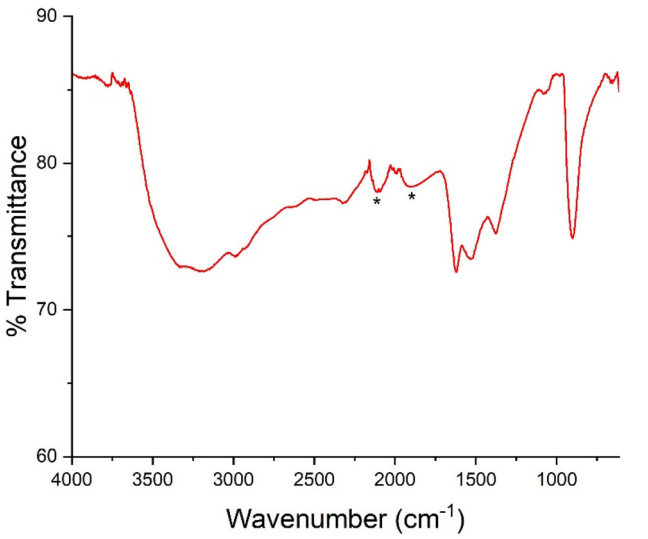

Fig. 5 FTIR spectrum of an oxide obtained through hydrothermal treatment (during 24 h, at 250 °C, with an initial pH = 8). Two bands, pointed out by asterisks, do not correspond to any carboxylate bands, as they are artefacts present in all our spectra.

Finally, the bands at 1530 and 1620 cm^{-1} result from the stretching mode of COO in carboxylate groups.[54] Therefore, we supposed the residual carbon to be present either as remaining oxalates, or as formiates, the latter being reported as a product of the hydrothermal decomposition of oxalate. Moreover, one must note that, between 3000 and 3500 cm^{-1} one broad band corresponding to the symmetric vibration of OH bands in water is observed, meaning that the oxide samples are still hydrated after drying in an oven at 90 °C overnight.

In order to quantify the presence of water within the samples, oxide powders obtained after hydrothermal conversion were also subjected to TG analysis. Two weight losses were observed, the first one from ambient temperature to 300–350 °C and the second one from 350 to 550 °C (Fig. S2†). Coupled mass spectrometry analyses showed that the weight losses observed during the thermal treatment correspond to the release of water, carbon monoxide and carbon dioxide during the first weight loss and only water during the second one. To calculate the water content, the weight loss corresponding to the carbon species was then subtracted to the total weight loss. As such, the water content of the oxides was found to be nearly constant as a function of the pH, remaining around 0.5 mole of water per mole of oxide. These contents are slightly higher than those obtained by Manaud *et al.*[19,20] for thorium and uranium simple oxides. Thus, cerium incorporation in the UO_2 structure appears to significantly alter the decomposition kinetics of organic species during conversion.

4.2. Effect of hydrothermal treatment duration

Another set of experiments was performed to investigate the impact of kinetics on the physico-chemical properties of the mixed uranium–cerium oxide samples obtained through the hydrothermal conversion of mixed uranium(IV)–cerium(III) oxalates. To do so, the heat treatment temperature was maintained at 250 °C while the initial pH value was fixed to 8. This latter guarantees a quantitative precipitation of both cations and leads to the formation of nano-powders, which generally present an increased reactivity during sintering.[55]

4.2.1. Precipitation yield and chemical composition. As before, ICP-OES analyses have been carried out on the supernatants to evaluate the impact of kinetics on the precipitation yields of the cations (Table 3). The precipitation yield of both cations after the oxalic precipitation is at least equal to 95%, in good agreement with the data generally reported for oxalic precipitation in the literature.[4,20] Conversely, after 1 h of hydrothermal treatment, the cerium precipitation appears to be quantitative while the uranium precipitation yield only reaches 88%. This difference is remarkable and reflects different kinetics of precipitation of both cations in the final oxide phase. Indeed, as the initial oxalate was found to be single phase and homogeneous, its dissolution is most likely to release both cations with the same kinetics. Therefore, conversion appears incomplete after 1 hour of hydrothermal treatment. Hence, the difference can only be explained by a faster hydrolysis of cerium in solution. Moreover, as hydrolysis of tetravalent cations is known to be more important than that of trivalent ones (considering the following sequence: $MO_2^+ < M^{3+} < MO_2^{2+} < M^{4+}$),[56] this can be seen as a first insight on the redox state of cerium at this step of the conversion. Indeed, if cerium would have remained trivalent in solution, its precipitation yield would have been less important than that obtained for uranium. Then, cerium oxidation probably occurs before being precipitated, and $Ce(OH)_4$ should be the most predominant form. Nevertheless, from 2 h of hydrothermal treatment, the precipitation yield appears quantitative and constant whatever the treatment time and the cation considered. Indeed, the results reported in Table 3 show that whatever the hydrothermal treatment time, the solid phases present the expected cationic molar ratio (*i.e.*, 80 at% of uranium and 20 at% of cerium). These results are consistent with the precipitation yields discussed above, even for 1 hour of hydrothermal treatment where the results might appear to be counter-intuitive. Indeed, if 90% of uranium and 99% of cerium are present in the solid phase, the ratio would still be equal to 78% of uranium and 22% of cerium. Moreover, when considering the uncertainty associated with the molar ratio given in Table 3, the results can be considered as consistent. As such, ICP-OES analyses showed that the hydrothermal treatment time does not affect significantly the composition of the final oxide.

Table 3 Determination of the cations precipitation yields and cationic stoichiometry (after powder dissolution in aqua regia) from ICP-OES analyses for various hydrothermal treatment times (T = 250 °C, pH = 8)

Hydrothermal treatment time (h)	Uranium precipitation yield (%)	Cerium precipitation yield (%)	U/(U + Ce) molar ratio[a] (%)	Ce/(U + Ce) molar ratio[a] (%)
Starting Oxalate	95 ± 2	98 ± 2	79 ± 2	21 ± 2
1	88 ± 2	99 ± 2	79 ± 2	21 ± 2
2	98 ± 2	99 ± 2	81 ± 2	19 ± 2
3	98 ± 2	99 ± 2	76 ± 2	24 ± 2
4	98 ± 2	99 ± 2	80 ± 2	20 ± 2
5	98 ± 2	99 ± 2	81 ± 2	19 ± 2
7	98 ± 2	99 ± 2	81 ± 2	20 ± 2
20	98 ± 2	99 ± 2	79 ± 2	21 ± 2
24	99 ± 2	99 ± 2	81 ± 2	19 ± 2
40	99 ± 2	99 ± 2	79 ± 2	21 ± 2
48	99 ± 2	99 ± 2	79 ± 2	21 ± 2

[a] Molar ratios determined from concentrations measured in solution after full dissolution in aqua regia.

4.2.2. Structural characterisation of the samples. Fig. 6 shows the XRD patterns obtained for samples prepared for various treatment times. It clearly shows that after 1 h of hydrothermal treatment, the solid obtained is polyphasic. Indeed, the XRD lines of the fluorite structure of U and Ce dioxides are evidenced, along with another unidentified phase exhibiting peaks for $2\theta < 20°$. These latter are likely to be caused by carboxylate species derived from the hydrothermal decomposition of oxalate[57] (or the oxalate itself), showing that this process remains incomplete after 1 h. However, the XRD pattern shows no extra peak characteristic of the sesquioxide Ce_2O_3, which once again goes in favour of the rapid oxidation of Ce^{3+} after the decomposition of the initial oxalate precursor.

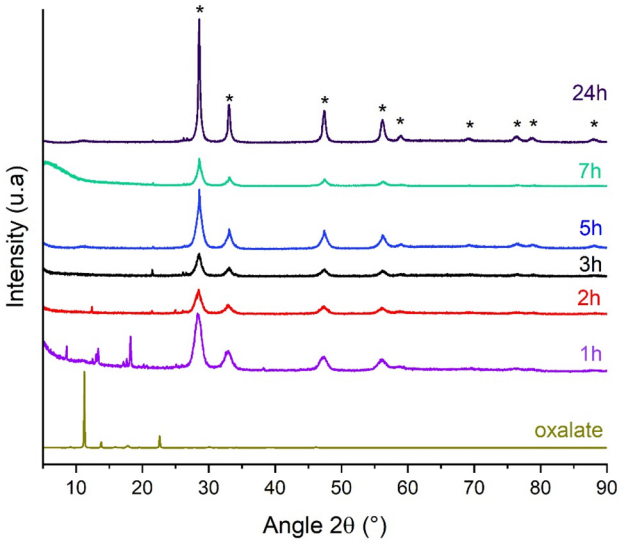

Fig. 6 Evolution of the XRD patterns obtained for samples prepared by the hydrothermal conversion of the initial mixed uranium–cerium oxalate from 1 to 24 hours (pH = 8, T = 250 °C). XRD lines associated with $U_{0.79}Ce_{0.21}O_2$ are pointed out by asterisks.[44]

Finally, no peak-splitting is noticeable, meaning that cerium and uranium already formed an unique mixed oxide phase $U_{1-x}Ce_xO_{2+\delta}{\cdot}nH_2O$. Whatever the time considered after 2 h, the fluorite structure is always obtained. XRD lines associated with secondary phases can be observed until 3 h of treatment, but one can note that the phase obtained for 2 h is different from the one obtained after 1 h. Indeed, after 2 h a single peak around 13° can be observed, corresponding to an unidentified phase coming from oxalate decomposition. For holding times longer than 3 h, fluorite is the only structure obtained even though a few peaks can appear on a recurring basis, around 2θ = 21.5 and 26°, caused by the presence of trace amounts of Ce-doped U_3O_8.[42,43] Therefore, 3 hours of hydrothermal treatment are required to fully convert oxalate into oxide.

Fig. 7 displays the evolution of the unit cell volume and the average crystallite size of mixed uranium–cerium oxides (considered as a single fluorite structure) during the hydrothermal treatment at 250 °C with an initial pH = 8. Both the results follow the same trend, with an increase from 2 to 7 h, before reaching a plateau. As such, the unit cell volume increases from approximately 159.75 Å^3 after 2 h to around 160.75 Å^3 for 7 hours. Meanwhile, the average crystallite size grows from around 10 nm to 17 nm when extending the holding time of the hydrothermal treatment from 1–2 h to 7 h. After 24 hours of hydrothermal treatment, no further modifications occurred, thus evidencing that oxalate conversion was complete and that the subsequent oxide phase reached thermodynamic equilibrium.

4.2.3. Homogeneity of the prepared samples. In order to assess the impact of hydrothermal treatment time on the cationic homogeneity in the oxide, the evolution of cerium distribution within the samples is presented in Fig. 8.

One can notice that, for the initial mixed oxalate, the sample is clearly homogeneous with 95% of the values included in ±4% around the average cerium content. After 1 h of hydrothermal treatment, the sample is way less homogeneous, as evidenced in the inset, and characterised by a broad distribution of cerium within the sample, with some areas of the pellet containing mainly cerium. As such, to account for 95% of the values, the interval is ten times larger than for the oxalate sample, *i.e.*, 40%. This result is in good agreement with previous XRD analyses, which have shown that after 1 h of treatment the sample obtained was polyphasic. Nevertheless, after 2 h of treatment the oxide exhibits a better homogeneity, with a 2σ interval varying slightly over the hydrothermal treatment time, as shown by the similar values collected, close to ±5%. Hence, as soon as the fluorite structure becomes predominant (t > 2 h), the oxide is homogeneous

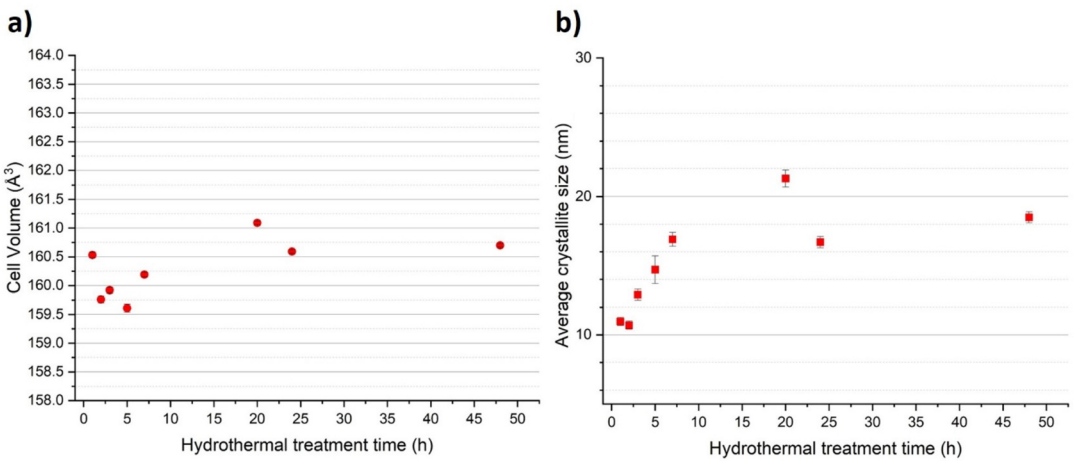

Fig. 7 Evolution of (a) the cell volume and (b) the average crystallite size of mixed uranium–cerium oxide (as a single fluorite-type structure) as a function of hydrothermal treatment duration (pH = 8, 250 °C).

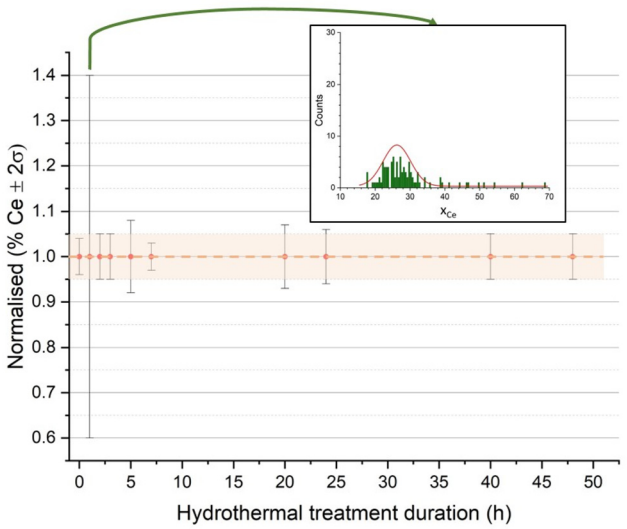

Fig. 8 Evolution of cationic homogeneity within the samples obtained by the hydrothermal conversion of oxalates as a function of the hydrothermal treatment duration, and the inset shows the wide cerium distribution in the oxide obtained after 1 h. Data at 0 h correspond to the initial oxalate. The orange area shows the homogeneity of an oxide prepared through thermal treatment (1000 °C, 6 h, Ar/H_2-4% atmosphere).

with the largest interval not exceeding ±8% of the average cerium content.

4.2.4. Morphology of the samples. SEM micrographs in SE mode and TEM-EDS images have also been recorded to address the effect of hydrothermal treatment time on the oxide morphology (Fig. 9). Three durations have been selected based on the previous results, *i.e.*, (i) 1 h to check how the presence of residual carboxylate within the oxide can affect the morphology and the homogeneity; (ii) 5 h to evidence the morphology of the single phase oxides formed for short hydrothermal treatment times; (iii) 24 hours to address on the morphology and homogeneity once a steady state is reached (which correspond to the micrograph for pH = 8 in Fig. 4).

In spite of the different results obtained from XRD analyses, SEM micrographs show that all the oxides studied present the same pattern composed of nanocrystallite agglomerates whatever the hydrothermal treatment duration considered. The platelet-like morphology of the initial oxalate is no longer visible, meaning that the initial oxalate has evolved, either as a less hydrated phase or as a decomposition product. This observation is thus in good agreement with the peaks located at 20° in the XRD pattern, which do not correspond to oxalate (Fig. 6).

The TEM-EDS results also show that after one hour of hydrothermal treatment, the sample obtained is composed of nanocrystallites containing both uranium and cerium. No uranium-or cerium-enriched spots are visible in the micrographs, which is surprising with regards to the SEM-EDS results obtained in Fig. 8, where the confidence level containing 95% of the values was larger than the other one (40% for 1 h, around 5% for other holding times). One must keep in mind that these TEM-EDS micrographs do not allow quantification of the chemical composition but are simply used to assess the presence of crystallites/areas enriched in one cation or another. Nevertheless, these results show that even the less homogeneous oxide obtained through hydrothermal conversion does not present an important heterogeneity, since all the crystallites are composed of uranium and cerium. Then, for 5 and 24 h of hydrothermal treatment, the results are similar, *i.e.* each nanocrystallite is composed of both cations and no change is noted from 1 to 24 h.

4.2.5. Carbon and water contents in the prepared samples. Carbon analyses were performed on oxides to investigate the role of the hydrothermal holding time on the carbon content in the samples (Table 4). In agreement with the XRD data, the carbon analyses show that after 1 h of hydrothermal treatment the samples still contain important amounts of carbon, probably coming from the presence of decomposition by-products. After 3 h of hydrothermal treatment, the carbon rate decreases down from 2.64 to 0.37 wt% and does not seem to change greatly when increasing the hydrothermal treatment time. Indeed, from 3 to 48 hours, the carbon rate remains below 0.52 wt%.

In parallel, the TGA results (Table 4) highlight that the oxide is close to be monohydrated after 1 h of hydrothermal treatment. During the conversion process, it is likely that cations were precipitated either as hydroxides or mixed oxy/hydroxy-carboxylate species. These precursor nuclei further age into hydrated oxide which gradually loss water with time. Such a mechanism is consistent with the formation of anhydrous actinide oxides as frequently reported in the literature[11,58] as follows:

$$An^{4+} + 4OH^- \rightarrow AnO_2 \cdot xH_2O + (2-x)H_2O \rightarrow AnO_2. \quad (1)$$

4.3. Variation of the oxide stoichiometry

In order to obtain optimal conditions for the conversion of oxalate into oxide regarding the holding time, the selected hydrothermal treatment time was fixed to 24 h to obtain a mixed oxide, showing the residual carbon and hydration rate as low as possible. Therefore, the last set of experiments performed in this paper focused on various cation stoichiometries. Five mixed oxide samples were prepared with x_{Ce} = 10, 20, 35, 50 and 75 at% of cerium. It is important to stress out that several studies[4,59] reported that the coprecipitation of An(IV)–Ln(III) oxalate leads to a solid solution exhibiting three different structures (hexagonal, quadratic or triclinic) as a function of the stoichiometry in trivalent cation.

4.3.1. Precipitation yield and chemical composition. ICP-OES analyses show that the precipitation of both cations is quantitative and congruent (Table 5), with a similar precipitation yield for uranium and cerium. Whatever the composition targeted, more than 94% of uranium and 97% of cerium are precipitated. Hence, precipitation yields do not vary significantly with pH or oxide stoichiometry, and are mainly impacted by the hydrothermal treatment duration.

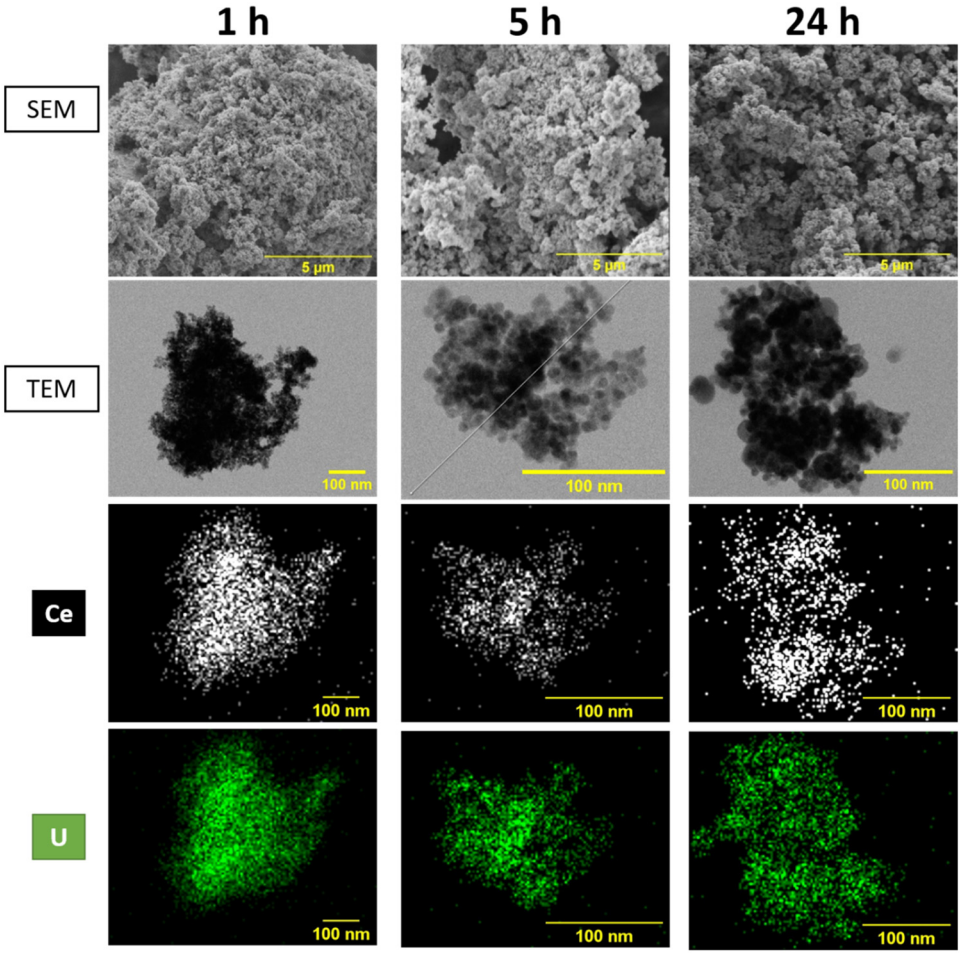

Fig. 9 SEM (SE mode) and TEM micrographs recorded for $U_{1-x}Ce_xO_{2+\delta}$ samples obtained after the hydrothermal treatment of mixed uranium–cerium oxalate (T = 250 °C, pH = 8) after various hydrothermal holding times; TEM-EDS analyses carried out on oxide samples obtained after different hydrothermal holding times (T = 250 °C, pH = 8).

Table 4 Carbon (wt%) and water (mol mol^{-1} cation) contents determined in the oxides as a function of the hydrothermal conversion of oxalates (pH = 8, T = 250 °C)

Hydrothermal holding time (h)	Carbon (wt%)	mol H_2O/mol cation
1	2.64 ± 0.05	1.0 ± 0.1
3	0.37 ± 0.05	0.5 ± 0.1
5	0.40 ± 0.05	0.7 ± 0.1
20	0.34 ± 0.05	0.8 ± 0.1
24	0.52 ± 0.05	0.6 ± 0.1
40	0.34 ± 0.05	0.3 ± 0.1
48	0.40 ± 0.05	0.3 ± 0.1

Table 5 Cation precipitation yields and obtained oxide stoichiometry for samples prepared using the hydrothermal conversion of oxalates (pH = 8, T = 250 °C, t = 24 h)

Expected stoichiometry	Uranium precipitation yield (%)	Cerium precipitation yield (%)	U/(U + Ce) molar ratio[a] (%)	Ce/(U + Ce) molar ratio[a] (%)
$U_{0.90}Ce_{0.10}O_{2\pm\delta}$	98 ± 2	98 ± 2	90 ± 2	10 ± 2
$U_{0.80}Ce_{0.20}O_{2\pm\delta}$	99 ± 2	99 ± 2	81 ± 2	19 ± 2
$U_{0.65}Ce_{0.35}O_{2\pm\delta}$	96 ± 2	98 ± 2	65 ± 2	35 ± 2
$U_{0.50}Ce_{0.50}O_{2\pm\delta}$	94 ± 2	97 ± 2	52 ± 2	48 ± 2
$U_{0.25}Ce_{0.75}O_{2\pm\delta}$	96 ± 2	99 ± 2	43 ± 2	57 ± 2
$U_{0.25}Ce_{0.75}O_{2\pm\delta}$ (36 h)	N.D	N.D	28 ± 2	72 ± 2

[a] Molar ratios determined from concentrations measured in solution after full dissolution in aqua regia.

All the samples prepared with up to 50% in cerium present the expected stoichiometry. Conversely, an atomic percentage of cerium equal to 57% was determined for an expected composition of $U_{0.25}Ce_{0.75}O_2$. As a result, the molar ratio calculated does not match with the precipitation yield determined. The most likely hypothesis is that undissolved cerium must be found in a phase that is refractory to dissolution, such as cerium(IV) oxide,[60,61] which would have precipitated during hydrothermal conversion.

An hydrothermal treatment of 36 hours was then performed, with the aim to incorporate quantitatively the cerium within the mixed oxide. This modified protocol led to an oxide presenting a stoichiometry close to the expected one, with a

Ce/(U + Ce) ratio of 0.72, which highlights different conversion kinetics of oxalates as a function of their cerium content and their crystal structure.

4.3.2. Structural characterisation of the samples. XRD analyses (Fig. 10) confirm that only the fluorite structure characteristic of An(IV)O_2 is obtained whatever the stoichiometry considered. On the other hand, no peak splitting can be observed in the diffractogram corresponding to $U_{0.43}Ce_{0.57}O_{2+\delta}$, indicating that the secondary phase containing cerium (probably CeO_2) is amorphous.

To assess the structural changes with the variation of stoichiometry, Rietveld refinements were carried out considering only one phase contribution (Fig. 11), following the reasoning developed in the previous sections. From x_{Ce} = 0.1 to 0.5, the unit cell volume decreases linearly with the cerium incorporation rate, in good agreement with the ionic radii of U^{4+} (1.00 Å) and Ce^{4+} (0.97 Å) in the eight-fold coordination.[62] Such a linear variation confirms the formation of a solid solution in the mentioned range of composition. Nonetheless, cell volumes appears to be systematically lower than the data reported in the literature,[43,63] which indicates that the obtained oxides exhibit a O/M ratio higher than 2.00. This phenomenon could be explained by the uranium (IV) propensity to oxidise in air,[63] and will be discussed further in this paper. For x_{Ce} > 0.5, but the trend bends towards the values obtained for the (U,Ce)$O_{2.00}$ samples. As such, with increasing cerium content, the mixed oxides exhibit a less important hyper-stoichiometry, in good agreement with the U–Ce–O ternary phase diagram. Also, it is important to recall that such a continuous variation of the unit cell parameter remains compatible with the Vegard's law, and the formation of solid solutions. Meanwhile, the average crystallite size appears to be poorly impacted by the chemical composition, with values typically between 20 and 40 nm, although a maximum was observed for $U_{0.43}Ce_{0.57}O_{2+\delta}$, but probably on a random basis.

4.3.3. Carbon and water contents in the prepared samples. Finally, carbon and thermogravimetric analyses were performed to assess the impact of stoichiometry on both carbon and water contents within the obtained mixed oxides (Table 6). The carbon content seems to increase with the cerium incorporation rate in the oxides. Indeed, both $Ce_{0.10}U_{0.90}O_{2\pm\delta}$ and $Ce_{0.20}U_{0.80}O_{2\pm\delta}$ appear to contain roughly the same amount of carbon (around 0.5 wt%) while this amount increases up to 0.7 wt% for higher Ce/(U + Ce) ratios. Moreover, all the oxides prepared were found to contain less than one mole of water. The hydration rate remains between 0.3 and 0.6 mol of water per mole of cation. Overall, analyses

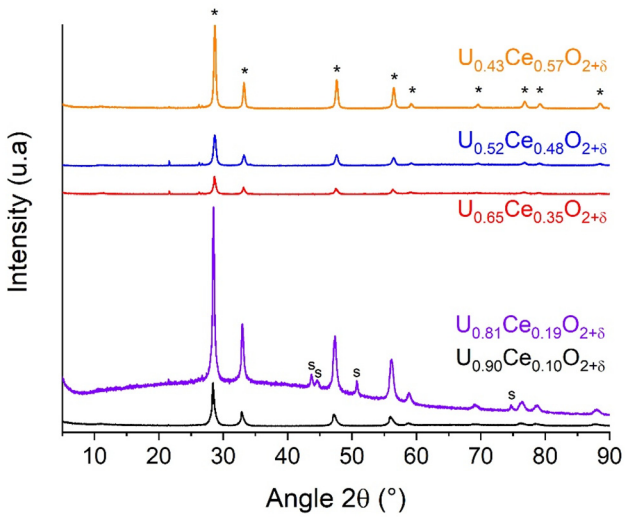

Fig. 10 Variation in the XRD patterns obtained for oxide samples prepared with different stoichiometries (pH = 8, T = 250 °C, t = 24 h). XRD peaks of $U_{0.79}Ce_{0.21}O_2$ [44] and the sample holder (austenite, PDF file 00-023-0298) are pointed by "*" and "s", respectively.

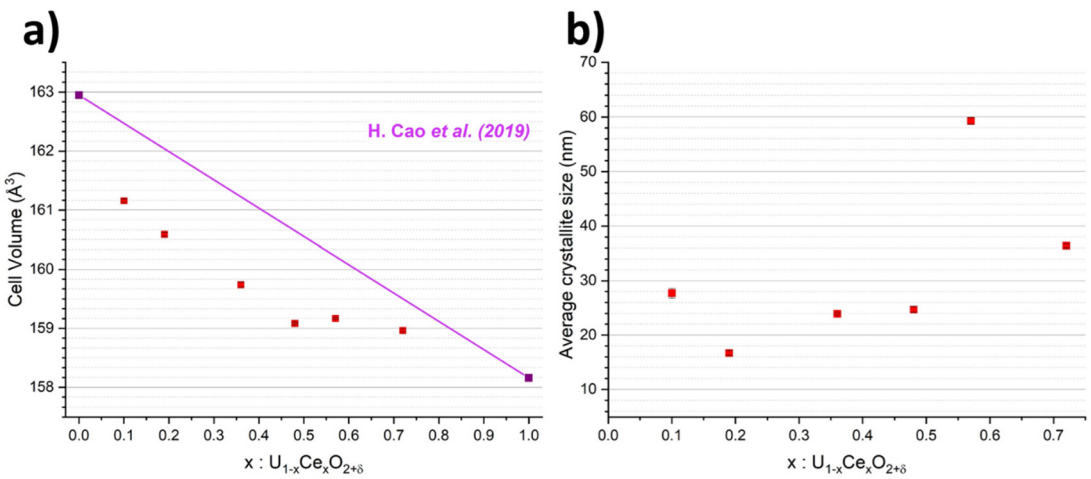

Fig. 11 Variation in (a) the unit cell volume, with the Vegard's law[45] between UO_2 and CeO_2 plotted in purple, and (b) the average crystallite size of mixed uranium–cerium oxide (as a single fluorite-type structure) as a function of the starting stoichiometry (hydrothermal treatment: pH = 8, T = 250 °C, t = 24 h).

Table 6 Carbon (wt%) and water (mol mol^{-1} cation) contents in the prepared oxides (T = 250 °C, t = 24 h, pH = 8).

Oxide stoichiometry	Carbon (wt%)	mol H_2O/mol cation (wt%)
$U_{0.90}Ce_{0.10}O_{2\pm\delta}$	0.47 ± 0.05	0.6 ± 0.1
$U_{0.81}Ce_{0.19}O_{2+\delta}$	0.52 ± 0.05	0.6 ± 0.1
$U_{0.65}Ce_{0.35}O_{2+\delta}$	0.60 ± 0.05	0.4 ± 0.1
$U_{0.52}Ce_{0.48}O_{2+\delta}$	0.62 ± 0.05	0.3 ± 0.1
$U_{0.43}Ce_{0.57}O_{2+\delta}$	0.70 ± 0.05	0.5 ± 0.1

performed show that the oxides synthesised present similar properties whatever the cerium content considered.

5. Discussion

As it was described before, precipitation yields of both elements were quantitative for the majority of the studied experimental conditions. This is unexpected considering the valence of precipitated cations within oxalate-based precursors. Indeed, in the hypothesis of a complexation by hydroxide anions, M(IV) and M(III) exhibit different hydrolysis kinetics, as it was reported by Choppin.[56] Moreover, as no extra peak than the fluorite ones are detected in the XRD patterns, it is likely that cerium(III) is oxidised during the hydrothermal process. Thus, it is mandatory to investigate how valence change could affect hydroxide precipitation yields, then the further conversion into oxide.[11] Therefore, the behaviour of uranium(IV), cerium(IV) and cerium(III) regarding to hydrolysis must be considered carefully, thanks to their associated solubility constants, allowing the determination of saturation indexes (I_S) in the solutions. Indeed, speciation differences between U^{4+}, Ce^{3+} and Ce^{4+} are expected due to different ionic potentials (*i.e.* charge over cationic radius ratio). It can induce different interactions with surrounding ligands, including hydroxide anions.[64] As such, significant differences in terms of hydrolysis are expected for the considered cations in the studied pH range.[65]

Consequently, thermodynamic calculations have been carried out to evaluate saturation indexes I_S associated with the hydrolysis of U^{4+}, Ce^{4+} and Ce^{3+}. The hydroxide precipitation reaction is usually defined as:

$$M(OH)_n \overset{K_{s,0}}{\longleftrightarrow} M^{n+} + nOH^- (\text{with } M^{n+} = U^{4+}, Ce^{4+}, Ce^{3+}) \quad (2)$$

according to Guillaumont *et al.*[66], the expression of associated solubility constant $K_{s,0}$ is thus:

$$K_{s,0} = [M^{n+}][OH^-]^n \quad (3)$$

where $[M^{n+}]$ and $[OH^-]$ stand for concentrations in solution. Moreover, Guillaumont *et al.*[66] also defined the complexation constant β_n, directly linked to $K_{s,0}$, as follows:

$$\beta_n = \frac{1}{[M^{n+}][OH^-]^n} = \frac{1}{K_{s,0}}. \quad (4)$$

All the β_n constants associated with U^{4+}, Ce^{4+} and Ce^{3+} are gathered in Table 7.

Table 7 Hydrolysis equilibria for considered cations and related $\log \beta_n$ as reported or calculated using the data from the literature

Considered equation	$\log \beta_n$	Ref.
$U^{4+} + 4OH^- \xrightarrow{\beta_4} U(OH)_{4(aq)}$	46.0	67
$Ce^{4+} + 4OH^- \xrightarrow{\beta_4} Ce(OH)_{4(aq)}$	47.5	Calculated from ref. 35
$Ce^{3+} + 3OH^- \xrightarrow{\beta_3} Ce(OH)_{3(aq)}$	14.8	

From elemental concentrations in solution, the I_S values have been determined as follows:

$$I_S = \log \frac{[M^{n+}] \times [OH^-]^n}{K_{s,0}}. \quad (5)$$

As such, the precipitation of solid species is favoured for $I_S > 0$. Even if thermodynamic data associated with hydrothermal conditions are extremely scarce, calculations under standard conditions and at room temperature can still help to approach the chemical behaviour of the considered elements under our conditions. During this study, the initial concentrations of the cations were set to $[U]_i = 2 \times 10^{-2}$ mol L^{-1} and $[Ce]_i = 5 \times 10^{-3}$ mol L^{-1}. Moreover, we chose to make these calculations under optimal conditions (*i.e.* pH = 8) as reported in Table 8.

First, it is noticeable that saturation index of U^{4+} is strongly positive, which means that the solution is largely oversaturated regarding to uranium tetrahydroxide. This finding implies that the concentration of uranium(IV) in solution is very low, which may appear to contradict the hypothesis of a dissolution/precipitation mechanism. Nevertheless, it is important to bear in mind that the thermodynamic data considered were obtained at room temperature. It is therefore likely that the solubility of U(IV) increases with the temperature considered in this work (T = 250 °C). Furthermore, previous work,[20] as well as the data obtained during this study, tends to show that uranium, initially tetravalent in the oxalate phase, is partially oxidised during the decomposition of the precursor (see next paragraphs focusing on the O/M ratio in the final precipitates). As such, the presence of U(VI) in solution cannot be ruled out, which de facto increases the total uranium concentration, making it possible to hypothesise an oxidative dissolution/reductive precipitation mechanism.

Regarding cerium, one must focus both on $Ce(OH)_3$ and $Ce(OH)_4$ saturation indexes computed aforementioned. Calculations have been performed for pH = 8 and considering that cerium was fully tetravalent in a first case, and trivalent in

Table 8 Determination of saturation indexes for hydrolysis equilibria regarding considered cations at pH = 8

Considered cation	[Cation] (mol L^{-1})	[OH^-] (mol L^{-1})	Saturation index I_S
U^{4+}	2×10^{-2}	10^{-6}	20.3
Ce^{4+} [a]	5×10^{-3}		21.2
Ce^{3+} [a]	5×10^{-3}		−5.5

[a] Considering that cerium is either fully tetravalent or trivalent.

a second case. From these calculations, the solution would be oversaturated (I_S = 21.2 ≫ 0) regarding to $Ce(OH)_4$ and undersaturated (I_S = −5.5 < 0) regarding to $Ce(OH)_3$. As cerium was found to be rapidly and quantitatively precipitated (for hydrothermal treatment duration as low as 1 h), thermodynamic calculations suggest that cerium(III) present in the starting oxalate precursor has been rapidly and quantitatively oxidised in solution during the conversion process. It can explain why no extra XRD line corresponding to the sesquioxide Ce_2O_3 was detected all along this study, whatever the pH value and the holding time considered. This could be explained by the fact that the precipitation of $Ce(OH)_4$ and the associated disappearance of cerium(IV) in solution induce equilibrium displacement from cerium(III) to cerium(IV), in accordance with Le Chatelier's principle. Moreover, as the system is strongly oversaturated regarding $Ce(OH)_4$ and $U(OH)_4$, the rapid formation of nanometric crystallites is favoured. This latter point directly supports the observed average size of oxide crystallites already discussed in the Results section.

Thanks to the multiparametric study reported herein, the lattice parameter of uranium–cerium mixed oxides synthesised through hydrothermal conversion was determined for different cerium incorporation rates and chemical conditions. As described in the Results section, the values obtained in this work appear to be systematically lower than the data from the literature, which can be attributed to oxygen hyper-stoichiometric mixed uranium–cerium dioxides. For instance, when studying the impact of pH, the unit cell volume of the mixed oxide appears to vary from 160.45 ± 0.02 Å to 161.2 ± 0.1 Å, which lies significantly below the data reported by authors for samples of similar composition, although with O/M = 2.00 (162.593 Å (ref. 43)). Likewise, when studying effect of hydrothermal holding time on oxides structures, the cell volume was lower than the ones from the literature, with a maximum plateau around 160.75 $Å^3$. Finally, the same observation was made when studying cerium stoichiometry variation within the oxides: cell volumes followed a linear trend similar to the Vegard's law between pure UO_2 and CeO_2 but with values systematically below those reported in the literature for stoichiometric compounds.[63,68]

In order to address this hyper-stoichiometry, calculations were carried out using Sali's equation,[43] which links the lattice parameter of uranium–cerium mixed oxides (a, expressed in Å) and cerium stoichiometry (x_{Ce}) to the O/M ratio (2 + δ). This equation is as follows:

$$a(\text{Å}) = 5.4704 - 0.06\delta - 0.07x_{Ce}. \quad (6)$$

The results of these calculations are compiled in Table S1† for oxides synthesised with varying initial pH values, in Table S2† for those obtained with different hydrothermal treatments, and finally in Table S3† for those synthesised with different cerium stoichiometries. Graphical representations are shown in Fig. 12.

What strikes at first sight is that regardless of the experimental parameter studied, most of the oxide samples prepared during this study present O/M ratios above 2.30.[63] Nevertheless, one has to note that Sali's equation[43] is an empirical relationship developed for bulk materials, whereas Rietveld refinements show that oxides studied herein are nanometric materials. Therefore, O/M ratios calculated are most likely to be overestimated. Nevertheless, although semi-quantitative, these results provide valuable information on hydrothermal conversion mechanisms and redox state evolution of cations. As such, it is possible that a fraction of cerium, initially trivalent, was not oxidised during the conversion. The presence of cerium(III) in the solid then could lead to uranium oxidation from U(IV) to U(V) to balance the charge. In addition, uranium(IV) easily oxidises in air, especially when it is present in powder samples, the specific area being more important.[63,68]

Fig. 12a shows that O/M ratios are not really influenced by pH, as values remain close to 2.35 whatever the studied conditions. The results as a function of hydrothermal treatment time are much more interesting. Indeed, Fig. 12b shows that the O/M ratio increases from 2.35 after 1 h of conversion to reach a maximum of 2.54 after 5 h, after which the O/M ratio starts to decrease steadily to reach 2.32 after 48 h. Such results are in good agreement with the findings of Manaud *et al.*,[20,69] who showed, using HERFD-XANES analyses, that uranium undergoes complex redox processes during the hydrothermal conversion of oxalate precursors, with O/U ratios in the final oxides varying from 2.65 after 1 h and 2.45 after 5 h (T = 250 °C, pH = 5). Uranium oxalate conversion and uranium–cerium oxalate then appear to run through a similar path composed of two steps. The first one is the oxidative decomposition/dissolution of the initial oxalate precipitate, where uranium is tetravalent, resulting in the release of U(V) and/or U(VI) in solution. Afterwards, uranium reduction is triggered by the presence of organic moieties in solution, originating from oxalate decomposition. Nakashima *et al.*[70,71] described uranium reduction thanks to organic species present in geologic media, where uranyl cations are reduced to UO_2 by interacting with simple organic compounds (lignite, simple alcohols or others aliphatic hydrocarbons), at relatively low temperatures (100–200 °C). XRD analyses in Fig. 6, as well as impurities rates in Table 4, corroborate this hypothesis, as they confirm that organic compounds are still present within the solid in the first hours of hydrothermal treatment, and then they should also exist in the supernatant. Such an oxidative decomposition/reductive precipitation mechanism also explain why the final morphologies are so different from the initial platelet one.

Finally, Fig. 12c shows that the O/M ratio decreases steadily when varying the cerium incorporation from $U_{0.9}Ce_{0.2}O_{2.35}$ to $U_{0.28}Ce_{0.72}O_{2.05}$, which is in good agreement with the discussion in Fig. 11a, where the variation in cell volumes determined for x_{Ce} > 0.50 was closer to the data reported in the literature for oxygen-stoichiometric compounds. Moreover, this result is in perfect agreement with the U–Ce–O phase diagram,[26] which shows that the MO_{2+y} + $M_4O_{9-\delta}$ domain is reduced to the benefit of single phase MO_{2+y} when increasing the temperature and the cerium content, hence corresponding to a global decrease of O/M.

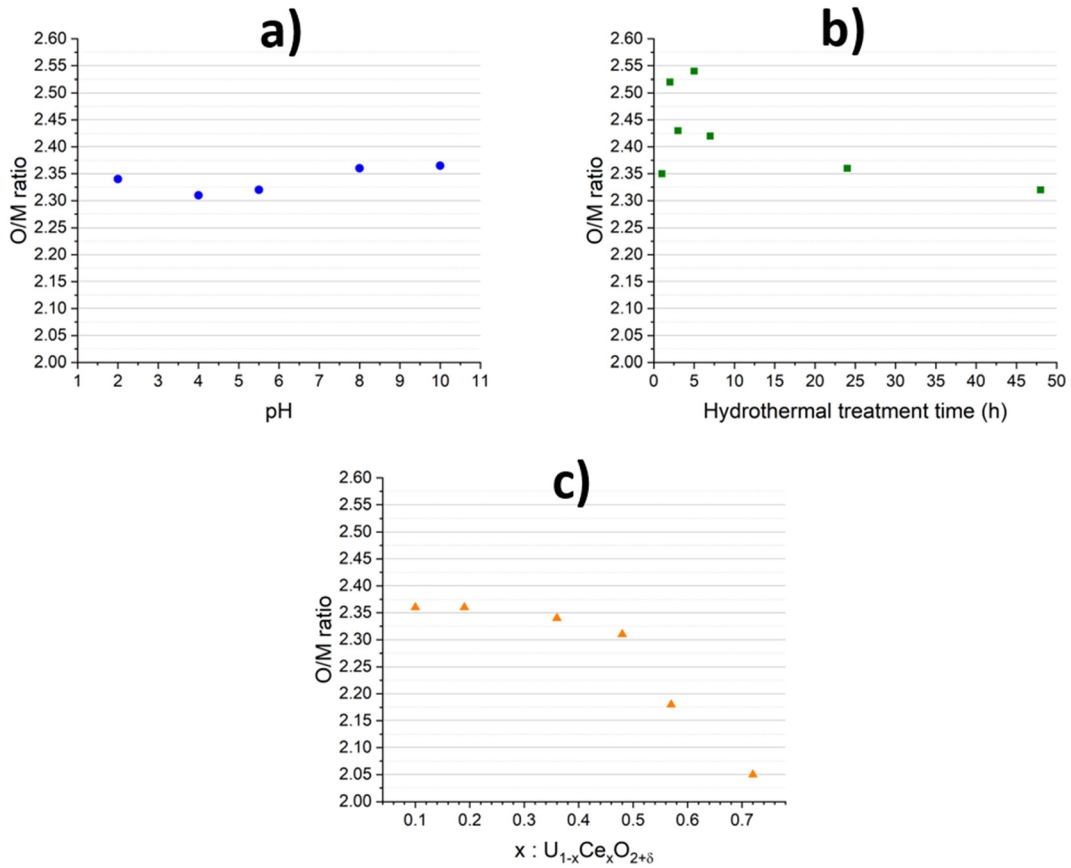

Fig. 12 Calculated O/M ratios using Sali's equation[43] as a function of pH (a); hydrothermal treatment time (b); x_{Ce} (c).

6. Conclusion

The hydrothermal conversion of uranium(IV)–cerium(III) oxalates into mixed uranium–cerium oxides $U_{1-x}Ce_xO_{2+\delta}{\cdot}nH_2O$ was investigated through a multi-parametric study to address the role of pH, hydrothermal treatment time and cerium content on the final properties of the oxides.

First, the pH of the initial reactive media was found to massively modify the morphology of the oxides that changed from nanospheres (pH = 2) to agglomerates of nanocrystallites (pH ≥ 8). The kinetics of the conversion process were then assessed by varying the hydrothermal treatment duration. After 1 h, the conversion appeared to be incomplete, which resulted in incongruent precipitation of uranium and cerium. Conversely, from 2 h and beyond, U and Ce precipitation was systematically found to be congruent and quantitative, with yields close to 99%. In parallel, the typical fluorite-type structure of $U_{1-x}Ce_xO_{2+\delta}{\cdot}nH_2O$ oxides was always detected by XRD, meaning that the oxalate conversion remained a rapid process. Also, the O/M ratio within the oxides prepared was found to decrease between 1 h and 7 h of hydrothermal treatment, which is consistent with a two-step conversion mechanism starting with the oxidative dissolution of the initial oxalate precursor, followed by a reductive precipitation into the oxide form.[20,69] Variation in the cerium stoichiometry was investigated at last. Above 50 at% in Ce, the modification of the structure of the initial precipitate led to a much slower hydrothermal decomposition.

The results obtained in this multi-parametric study then highlighted the complex chemical behaviour operating in our system under hydrothermal conditions, with several redox reactions occurring in the reactor, both in the solution and solid states, and each presenting different kinetics. Despite such an interplay in uranium and cerium behaviours, quantitative precipitation of highly homogeneous oxides was achieved, while some of the properties of the latter can be tuned when setting the treatment time or the pH of the initial media. As such, the optimal conditions for the conversion of uranium(IV)–cerium(III) oxalates into mixed uranium–cerium oxides $U_{1-x}Ce_xO_{2+\delta}{\cdot}nH_2O$ could be set to pH = 8, 24 hours of hydrothermal treatment time and $x_{Ce} < 0.5$, which allows one to quantitatively recover U and Ce as a reactive nanostructured powder that might be further easily sintered. The hydrothermal conversion of oxalates then appears to be a credible alternative route for the synthesis of mixed oxide nuclear fuels.

Author contributions

S. B.: conceptualisation; data acquisition; data analysis; writing the original draft; review; final approval. N. C.: con-

ception of the work; data analysis; validation; writing the original draft; review; final approval. N. D.: conceptualisation; data analysis; validation; writing the original draft; review; final approval. X. F. L., J. L. and L. D. M.: data acquisition; data analysis.

Conflicts of interest

The authors declare no competing interests.

Acknowledgements

The authors are grateful to Fatima Chmali and Maëva Munoz for their help during the synthesis and characterisation experiments. The authors would like to thank CEA for funding the PhD work of Sofian Benarib.

References

1 C. Poinssot, C. Rostaing, S. Greandjean and B. Boullis, Recycling the Actinides, The Cornerstone of Any Sustainable Nuclear Fuel Cycles, *Procedia Chem.*, 2012, **7**, 349–357, DOI: **10.1016/j.proche.2012.10.055**.

2 G. Oudinet, I. Munoz-Viallard, L. Aufore, M.-J. Gotta, J. M. Becker, G. Chiarelli and R. Castelli, Characterization of plutonium distribution in MIMAS MOX by image analysis, *J. Nucl. Mater.*, 2008, **375**(1), 86–94, DOI: **10.1016/j.jnucmat.2007.10.013**.

3 Z. Talip, S. Peuget, M. Magnin, M. Tribet, C. Valot, R. Vauchy and C. Jégou, Characterization of un-irradiated MIMAS MOX fuel by Raman spectroscopy and EPMA, *J. Nucl. Mater.*, 2018, **499**, 88–97, DOI: **10.1016/j.jnucmat.2017.11.014**.

4 F. Abraham, B. Arab-Chapelet, M. Rivenet, C. Tamain and S. Grandjean, Actinide oxalates, solid state structures and applications, *Coord. Chem. Rev.*, 2014, **266–267**(1), 28–68, DOI: **10.1016/j.ccr.2013.08.036**.

5 C. Tamain, Arab Chapelet B, Rivenet M, Abraham F, Caraballo R, Grandjean S. Crystal growth and first crystallographic characterization of mixed uranium(IV)-plutonium (III) oxalates, *Inorg. Chem.*, 2013, **52**(9), 4941–4949, DOI: **10.1021/ic302587t**.

6 S. Grandjean, B. Arab-Chapelet, A. C. Robisson, F. Abraham, Ph. Martin, J.-Ph. Dancausse, N. Herlet and C. Léorier, Structure of mixed U(IV)-An(III) precursors synthesized by co-conversion methods (where An=Pu, Am or Cm), *J. Nucl. Mater.*, 2009, **385**(1), 204–207, DOI: **10.1016/j.jnucmat.2008.10.039**.

7 B. Arab-chapelet, S. Grandjean, G. Nowogrocki and F. Abraham, Synthesis of new mixed actinides oxalates as precursors of actinides oxide solid solutions, *J. Alloys Compd.*, 2007, **445**, 387–390, DOI: **10.1016/j.jallcom.2007.01.033**.

8 D. Dollimore, The thermal decomposition of oxalates, *Thermochim. Acta*, 1987, **117**, 331–363, DOI: **10.1016/0040-6031(87)88054-1**.

9 N. Clavier, N. Hingant, M. Rivenet, S. Obbade, N. Dacheux, N. Barré and F. Abraham, X-ray diffraction and μ-raman investigation of the monoclinic - orthorhombic phase transition in $Th_{1-x}U_x(C_2O_4)_2 \cdot 2H_2O$ solid solutions, *Inorg. Chem.*, 2010, **49**(4), 1921–1931, DOI: **10.1021/ic902343r**.

10 L. Claparede, N. Clavier, A. Mesbah, F. Tocino, S. Szenknect, J. Ravaux and N. Dacheux, Impact of the cationic homogeneity on $Th_{0.5}U_{0.5}O_2$ densification and chemical durability, *J. Nucl. Mater.*, 2019, **514**, 368–379, DOI: **10.1016/j.jnucmat.2018.12.009**.

11 J. Martinez, N. Clavier, A. Mesbah, F. Audubert, X. F. Le Goff, N. Vigier and N. Dacheux, An original precipitation route toward the preparation and the sintering of highly reactive uranium cerium dioxide powders, *J. Nucl. Mater.*, 2015, **462**, 173–181, DOI: **10.1016/j.jnucmat.2015.03.053**.

12 N. Vigier, S. Grandjean, B. Arab-chapelet and F. Abraham, Reaction mechanisms of the thermal conversion of Pu(IV) oxalate into plutonium oxide, *J. Alloys Compd.*, 2007, **445**, 594–597, DOI: **10.1016/j.jallcom.2007.01.057**.

13 N. Hingant, N. Clavier, N. Dacheux, N. Barré, S. Hubert, S. Obbade, F. Taborda and F. Abraham, Preparation, sintering and leaching of optimized uranium thorium dioxides, *J. Nucl. Mater.*, 2009, **385**(2), 400–406, DOI: **10.1016/j.jnucmat.2008.12.011**.

14 J. Martinez, N. Clavier, T. Ducasse, A. Mesbah, F. Audubert, B. Corso, N. Vigier and N. Dacheux, From uranium(IV) oxalate to sintered UO_2: Consequences of the powders' thermal history on the microstructure, *J. Eur. Ceram. Soc.*, 2015, **35**(16), 4535–4546, DOI: **10.1016/j.jeurceramsoc.2015.07.010**.

15 C. Chambon, S. Vaudez and J. M. Heintz, De-densification mechanisms of yttria-doped cerium oxide during sintering in a reducing atmosphere, *J. Am. Ceram. Soc.*, 2018, **101**(11), 4956–4967, DOI: **10.1111/jace.15741**.

16 G. I. N. Bouala, N. Clavier, R. Podor, J. Cambedouzou, A. Mesbah, H.-P. Brau, J. Léchelle and N. Dacheux, Preparation and characterisation of uranium oxides with spherical shapes and hierarchical structures, *CrystEngComm*, 2014, **16**, 6944–6954, DOI: **10.1039/c4ce00850b**.

17 N. Clavier, J. Maynadié, A. Mesbah, J. Hidalgo, R. Lauwerier, G. I. Nkou Bouala, S. Parrès-Maynadié, D. Meyer, N. Dacheux and R. Podor, Thorium aspartate tetrahydrate precursor to ThO_2: Comparison of hydrothermal and thermal conversions, *J. Nucl. Mater.*, 2017, **487**, 331–342, DOI: **10.1016/j.jnucmat.2017.02.035**.

18 V. Trillaud, J. Maynadie, J. Manaud, J. Hidalgo, D. Meyer, R. Podor, N. Dacheux and N. Clavier, Synthesis of size-controlled UO_2 microspheres from the hydrothermal conversion of U (IV) aspartate, *CrystEngComm*, 2018, **20**, 7749–7760, DOI: **10.1039/C8CE01352G**.

19 J. Manaud, J. Maynadié, A. Mesbah, M. O. J. Y. Hunault, Ph. M. Martin, M. Zunino, N. Dacheux and N. Clavier, Hydrothermal Conversion of Thorium Oxalate into ThO_2·

nH_2O Oxide, *Inorg. Chem.*, 2020, **59**(20), 14954–14966, DOI: **10.1021/acs.inorgchem.0c01633**.

20 J. Manaud, J. Maynadié, A. Mesbah, M. O. J. Y. Hunault, Ph. M. Martin, M. Zunino, D. Meyer, N. Dacheux and N. Clavier, Hydrothermal Conversion of Uranium(IV) Oxalate into Oxides: A Comprehensive Study, *Inorg. Chem.*, 2020, **59**(5), 3260–3273, DOI: **10.1021/acs.inorgchem.9b03672**.

21 K. Popa, O. Walter, O. Dieste Blanco, A. Guiot, D. Bouëxière, J.-Y. Colle, L. Martel, M. Naji and D. Manara, A low-temperature synthesis method for AnO_2 nanocrystals (An=Th, U, Np, and Pu) and associate solid solutions, *CrystEngComm*, 2018, **20**(32), 4614–4622, DOI: **10.1039/c8ce00446c**.

22 O. Walter, K. Popa and O. D. Blanco, Hydrothermal decomposition of actinide(IV) oxalates: A new aqueous route towards reactive actinide oxide nanocrystals, *Open Chem.*, 2016, **14**(1), 170–174, DOI: **10.1515/chem-2016-0018**.

23 L. Balice, D. Bouëxière, M. Cologna, A. Cambriani, J.-F. Vigier, E. De Bona, G.D. Sorarù, C. Kübel, O. Walter and K. Popa, Nano and micro $U_{1-x}Th_xO_2$ solid solutions: From powders to pellets, *J. Nucl. Mater.*, 2018, **498**, 307–313, DOI: **10.1016/j.jnucmat.2017.10.042**.

24 G. Kauric, O. Walter, A. Beck, B. Schacherl, O. Dieste Blanco, J.-F. Vigier, E. Zuleger, T. Vitova and K. Popa, Synthesis and characterization of nanocrystalline $U_{1-x}Pu_xO_{2+y}$ mixed oxides, *Mater. Today Adv.*, 2020, **8**, 100105, DOI: **10.1016/j.mtadv.2020.100105**.

25 J. F. Vigier, D. Freis, O. Walter, O. Dieste Blanco, D. Bouëxière, E. Zuleger, N. Palina, T. Vitova, R. J. M. Konings and K. Popa, Synthesis and characterization of homogeneous $(U,Am)O_2$ and $(U,Pu,Am)O_2$ nanopowders, *CrystEngComm*, 2022, **24**(36), 6338–6348, DOI: **10.1039/d2ce00527a**.

26 T. L. Markin, R. S. Street and E. C. Crouch, The uranium-cerium-oxygen ternary phase diagram, *J. Inorg. Nucl. Chem.*, 1970, **32**(1967), 59–75.

27 H. S. Kim, C. Y. Joung, B. H. Lee, J. Y. Oh, Y. H. Koo and P. Heimgartner, Applicability of CeO_2 as a surrogate for PuO_2 in a MOX fuel development, *J. Nucl. Mater.*, 2008, **378**(1), 98–104, DOI: **10.1016/j.jnucmat.2008.05.003**.

28 R. Lorenzelli and B. Touzelin, Sur le système UO_2-CeO_2; étude cristallographique à haute température, *J. Nucl. Mater.*, 1980, **95**(3), 290–302, DOI: **10.1016/0022-3115(80)90371-2**.

29 W. Dörr, Study of the formation of UO_2-PuO_2 solid solution by means of UO_2-CeO_2 simulate, *J. Nucl. Mater.*, 1986, **140**, 7–10, DOI: **10.1016/0022-3115(86)90190-X**.

30 N. Dacheux, V. Brandel and M. Genet, Synthesis and properties of uranium chloride phosphate tetrahydrate: $UClPO_4{\cdot}4H_2O$, *New J. Chem.*, 1995, **19**, 1029–1036.

31 A. Rabenau, The Role of Hydrothermal Synthesis in Preparative Chemistry, *Angew. Chem., Int. Ed. Engl.*, 1985, **24**(12), 1026–1040, DOI: **10.1002/anie.198510261**.

32 B. H. Toby and R. B. Von Dreele, GSAS-II: The genesis of a modern open-source all purpose crystallography software package, *J. Appl. Crystallogr.*, 2013, **46**(2), 544–549, DOI: **10.1107/S0021889813003531**.

33 D. Rai, A. R. Felmy and J. L. Ryan, Uranium(IV) Hydrolysis Constants and Solubility Product of $UO_2 \cdot xH_2O$(am), *Inorg. Chem.*, 1990, **29**(2), 260–264, DOI: **10.1021/ic00327a022**.

34 B. Bouchaud, J. Balmain, G. Bonnet and F. Pedraza, PH-distribution of cerium species in aqueous systems, *J. Rare Earths*, 2012, **30**(6), 559–562, DOI: **10.1016/S1002-0721(12)60091-X**.

35 R. Marsac, F. Réal, N. L. Banik, M. Pédrot, O. Pourret and V. Vallet, Aqueous chemistry of Ce(IV): Estimations using actinide analogues, *Dalton Trans.*, 2017, **46**(39), 13553–13561, DOI: **10.1039/c7dt02251d**.

36 S. A. Hayes, P. Yu, T. J. O'Keefe, M. J. O'Keefe and J. O. Stoffer, The Phase Stability of Cerium Species in Aqueous Systems, *J. Electrochem. Soc.*, 2002, **149**(12), C623–C630, DOI: **10.1149/1.1516775**.

37 K. Opel, S. Weiß, S. Hübener, H. Zänker and G. Bernhard, Study of the solubility of amorphous and crystalline uranium dioxide by combined spectroscopic methods, *Radiochim. Acta*, 2007, **95**(3), 143–149, DOI: **10.1524/ract.2007.95.3.143**.

38 C. Tamain, B. Arab-Chapelet, M. Rivenet, F. Abraham and S. Grandjean, Single crystal synthesis methods dedicated to structural investigations of very low solubility mixed-actinide oxalate coordination polymers, *Cryst. Growth Des.*, 2012, **12**(11), 5447–5455, DOI: **10.1021/cg301039m**.

39 G. Leinders, T. Cardinaels, K. Binnemans and M. Verwerft, Accurate lattice parameter measurements of stoichiometric uranium dioxide, *J. Nucl. Mater.*, 2015, **459**, 135–142, DOI: **10.1016/j.jnucmat.2015.01.029**.

40 R. Schmitt, A. Nenning, O. Kraynis, R. Korobko, A. I. Frenkel, I. Lubormirsky, S. M. Haile and J. L. M. Rupp, A review of defect structure and chemistry in ceria and its solid solutions, *Chem. Soc. Rev.*, 2020, **49**(2), 554–592, DOI: **10.1039/c9cs00588a**.

41 R. Wang, P. A. Crozier and R. Sharma, Structural transformation in ceria nanoparticles during redox processes, *J. Phys. Chem. C*, 2009, **113**(14), 5700–5704, DOI: **10.1021/jp8107232**.

42 K. S. Kumar, T. Mathews, H. P. Nawada and N. P. Bhat, Oxidation behaviour of uranium in the internally gelated urania-ceria solid solutions - XRD and XPS studies, *J. Nucl. Mater.*, 2004, **324**(2–3), 177–182, DOI: **10.1016/j.jnucmat.2003.09.014**.

43 S. K. Sali, M. Keskar, R. Phatak, K. Krishnan, G. P. Shelke, P. P. Muhammed Shafeeq, S. Kannan, *et al.*, Oxidation behavior of $(U_{1-y}Ce_y)O_{2.00}$; (y=0.21, 0.28 and 0.44) solid solutions under different oxygen potentials. Thermogravimetric and in situ X-ray diffraction studies, *J. Nucl. Mater.*, 2018, **510**, 499–512, DOI: **10.1016/j.jnucmat.2018.08.043**.

44 W. Rüdorff and G. Valet, Über das Ceruranblau und Mischkristalle im System CeO_2-UO_2-U_3O_8, *Z. Anorg. Allg. Chem.*, 1953, **271**(5–6), 257–272, DOI: **10.1002/zaac.19532710504**.

45 H. Cao, H. Bao, X. Lin, J. Lin, L. Zhang, Y. Huang and J.-Q. Wang, Differential interplay between Ce and U on local structures of $U_{1-x}Ce_xO_2$ solid solutions probed by

X-ray absorption spectroscopy, *J. Nucl. Mater.*, 2019, **515**, 238–244, DOI: 10.1016/j.jnucmat.2018.12.042.

46 G. D. White, L. A. Bray and P. E. Hart, Optimization of thorium oxalate precipitation conditions relative to derived oxide sinterability, *J. Nucl. Mater.*, 1981, **96**(3), 305–313, DOI: 10.1016/0022-3115(81)90574-2.

47 L. Duvieubourg-Garela, N. Vigier, F. Abraham and S. Grandjean, Adaptable coordination of U(IV) in the 2D-(4,4) uranium oxalate network: From 8 to 10 coordinations in the uranium(IV) oxalate hydrates, *J. Solid State Chem.*, 2008, **181**(8), 1899–1908, DOI: 10.1016/j.jssc.2008.04.010.

48 V. Tyrpekl, P. Markova, M. Dopita, P. Brázda and M. A. Vacca, Cerium Oxalate Morphotypes: Synthesis and Conversion into Nanocrystalline Oxide, *Inorg. Chem.*, 2019, **58**(15), 10111–10118, DOI: 10.1021/acs.inorgchem.9b01250.

49 V. Tyrpekl, M. Beliš, T. Wangle, J. Vleugels and M. Verwerft, Alterations of thorium oxalate morphology by changing elementary precipitation conditions, *J. Nucl. Mater.*, 2017, **493**, 255–263, DOI: 10.1016/j.jnucmat.2017.06.027.

50 A. G. Shtukenberg, M. D. Ward and B. Kahr, Crystal growth inhibition by impurity stoppers, now, *J. Cryst. Growth*, 2022, **597**, 126839, DOI: 10.1016/j.jcrysgro.2022.126839.

51 A. B. Bard, X. Zhou, X. Xia, G. Zhu, M. B. Lim, S. M. Kim, M. C. Johnson, J. M. Kollman, M. A. Marcus, S. R. Spurgeon, D. E. Perea, A. Devaraj, J. Chun, J. J. De Yeoro and J. Pauzauskie, A Mechanistic Understanding of Nonclassical Crystal Growth in Hydrothermally Synthesized Sodium Yttrium Fluoride Nanowires, *Chem. Mater.*, 2020, **32**(7), 2753–2763, DOI: 10.1021/acs.chemmater.9b04076.

52 G. Mirabello, A. Ianiro, P. H. H. Bomans, T. Yoda, A. Arakaki, H. Friedrich, G. De With and N. A. J. M. Sommerdijk, Crystallization by particle attachment is a colloidal assembly process, *Nat. Mater.*, 2020, **19**(4), 391–396, DOI: 10.1038/s41563-019-0511-4.

53 K. Nakamoto, *Infrared and Raman Spectra of Inorganic and Coordination Compounds Part B: Applications in Coordination, Organometallic, and Bioinorganic Chemistry*, John Wiley & Sons Inc., 6th edn, 2009..

54 K. Ito and H. J. Bernstein, the Vibrational Spectra of the Formate, Acetate, and Oxalate Ions, *Can. J. Chem.*, 1956, **34**(2), 170–178, DOI: 10.1139/v56-021.

55 J. Manaud, R. Podor, X. F. Le Goff, J. Maynadié, N. Dacheux and N. Clavier, Direct sintering of UO_{2+x} oxides prepared under hydrothermal conditions, *J. Eur. Ceram. Soc.*, 2021, **41**(13), 6697–6707, DOI: 10.1016/j.jeurceramsoc.2021.06.006.

56 G. R. Choppin, Solution Chemistry of the Actinides, *Radiochim. Acta*, 1983, **32**(1–3), 43–54, DOI: 10.1524/ract.1983.32.13.43.

57 L. J. Crossey, Thermal degradation of aqueous oxalate species, *Geochim. Cosmochim. Acta*, 1991, **55**(6), 1515–1527, DOI: 10.1016/0016-7037(91)90124-N.

58 N. Clavier, Y. Cherkaski, J. Martinez, S. Costis, T. Cordara, F. Audubert, L. Brissonneau and N. Dacheux, Synthesis and Direct Sintering of Nanosized $(M^{IV}, M^{III})O_{2-x}$ Hydrated Oxides as Electrolyte Ceramics, *ChemPhysChem*, 2017, **18**, 2666–2674, DOI: 10.1002/cphc.201700647.

59 C. Tamain, S. Grandjean, B.A Chapelet and F. Abraham, Synthesis and structural characterisation of mixed An(IV) -An(III) actinide oxalates used as precursors for dedicated fuel or target, in *Proceedings of the First ACSEPT International Workshop*, 2010.

60 L. Claparede, N. Clavier, N. Dacheux, A. Mesbah, J. Martinez, S. Szenknect and Ph. Moisy, Multiparametric dissolution of thorium-cerium dioxide solid solutions, *Inorg. Chem.*, 2011, **50**(22), 11702–11714, DOI: 10.1021/ic201699t.

61 L. Joret, G. Cote and D. Bauer, Effect of microwaves on the rate of dissolution of metal oxides (Co_3O_4 and CeO_2) in nitric acid, *Hydrometallurgy*, 1997, **45**(1–2), 1–12, DOI: 10.1016/s0304-386x(96)00077-1.

62 R. D. Shannon, Revised effective ionic radii and systematic studies of interatomic distances in halides and chalcogenides, *Acta Crystallogr., Sect. A: Cryst. Phys., Diffr., Theor. Gen. Crystallogr.*, 1976, **32**(5), 751–767, DOI: 10.1107/S0567739476001551.

63 M. Massonet, L. Claparede, J. Martinez, Ph.M. Martin, M. O.J.Y. Hunault, D. Prieur, A. Mesbah, N. Dacheux and N. Clavier, Influence of sintering conditions on the structure and the redox speciation of homogenous $(U,Ce)O_{2+\delta}$ ceramics: a synchrotron study, *Inorg. Chem.*, 2023, **62**, 7173–7185, DOI: 10.1021/acs.inorgchem.2c03945.

64 G. R. Choppin, Actinide speciation in aquatic systems, *Mar. Chem.*, 2006, **99**(1–4), 83–92, DOI: 10.1016/j.marchem.2005.03.011.

65 B. A. Bilal and E. Müller, Thermodynamic Study of Ce^{4+}/Ce^{3+} Redox Reaction in Aqueous Solutions at Elevated Temperatures: 1. Reduction Potential and Hydrolysis Equilibria of Ce^{4+} in $HClO_4$ Solutions, *Z. Naturforsch., A: Phys. Sci.*, 1992, **47**(9), 974–984, DOI: 10.1515/zna-1992-0908.

66 R. Guillaumont, *Chemical Thermodynamics, Vol. 5, Update on the Chemical Thermodynamics of Uranium, Neptunium, Plutonium, Americium and Technetium, OECD Nuclear Agency*, Elsevier, 2003.

67 V. Neck and J. I. Kim, Solubility and hydrolysis of tetravalent actinides, *Radiochim. Acta*, 2001, **89**(1), 1–16, DOI: 10.1524/ract.2001.89.1.001.

68 D. Prieur, J. F. Vigier, K. Popa, O. Walter, O. Dieste, Z. Varga, A. Beck, T. Vitova, A. Scheinost and Ph. M. Martin, Charge Distribution in $U_{1-x}Ce_xO_{2+y}$ Nanoparticles, *Inorg. Chem.*, 2021, **60**(19), 14550–14556, DOI: 10.1021/acs.inorgchem.1c01071.

69 J. Manaud, *Conversion Hydrothermale d'oxalates d'actinides Tétravalents: De La Synthèse Au Frittage Des Poudres d'oxydes*, Ecole Nationale Supérieure de Chimie de Montpellier, 2020.

70 S. Nakashima, Kinetics and thermodynamics of U reduction by natural and simple organic matter, *Org. Geochem.*, 1992, **19**(4–6), 421–430, DOI: 10.1016/0146-6380(92)90009-M.

71 S. Nakashima, Complexation and reduction of uranium by lignite, *Sci. Total Environ.*, 1992, **117–118**(C), 425–437, DOI: 10.1016/0048-9697(92)90108-5.